Title

The Importance of Accounting for Landscape Position When Investigating Grasslands: A Multidisciplinary Characterisation of a California Coastal Grassland

Journal

Earth's Future, 12(6)

ISSN

2328-4277

Authors

Rowley, Mike C

Falco, Nicola

Pegoraro, Elaine

et al.

Publication Date

2024-06-01

DOI

10.1029/2023ef004208

Earth's Future

RESEARCH ARTICLE
10.1029/2023EF004208

Special Collection:
The Future of Critical Zone Science: Towards Shared Goals, Tools, Approaches and Philosophy

The Importance of Accounting for Landscape Position When Investigating Grasslands: A Multidisciplinary Characterisation of a California Coastal Grassland

Mike C. Rowley[1,2,3], Nicola Falco[2], Elaine Pegoraro[2], Baptiste Dafflon[2], Cynthia Gerlein-Safdi[2,4], Yuxin Wu[2], Cristina Castanha[2], Jasquelin Peña[2,3], Peter S. Nico[2,4], and Margaret S. Torn[2,4]

[1]University of Zurich, Zürich, Switzerland, [2]Lawrence Berkeley National Laboratory, Berkeley, CA, USA, [3]University of California, Davis, Davis, CA, USA, [4]University of California, Berkeley, Berkeley, CA, USA

Mike C. Rowley, Nicola Falco, Elaine Pegoraro, Cynthia Gerlein-Safdi, and Baptiste Dafflon contributed equally to this manuscript and shared the first authorship.

Abstract Grasslands are one of the most common land-cover types, providing important ecosystem services globally, yet few studies have examined grassland critical-zone functioning throughout hillslopes. This study characterised a coastal grassland over a small hillslope at Point Reyes National Seashore, California, using multidisciplinary techniques, combining remotely-sensed, geophysical, plant, and soil measurements. Clustering techniques delineated the study area into four landscape zones, up-, mid-, and down-slope, and a bordering riparian ecotone, which had distinct environmental properties that varied spatially across the site, with depth, and time. Soil moisture increased with depth and down slope towards a bordering riparian zone, and co-varied with soil CO_2 flux rates both spatially and temporally. This highlighted three distinct controls of soil moisture on soil respiration: CO_2 fluxes were inhibited by high moisture content in the down-slope during the wet winter months, and converged across landscape positions in the dry summer months, while also displaying post-rain pulses. The normalised difference vegetation index (NDVI) ranged from 0.32 (September)–0.80 (April) and correlated positively with soil moisture and aboveground biomass, moving down slope. Yet, NDVI, aboveground biomass, and soil moisture were not correlated to soil organic carbon (SOC) content (0.4%–4.5%), which was highest in the mid-slope. The SOC content may instead be linked to shifts in dominant grassland species and their rhizosphere properties with landscape position. This multidisciplinary characterisation highlighted significant heterogeneity in grassland properties with landscape position, and demonstrated an approach that could be used to characterise other critical-zone environments on hillslopes.

Plain Language Summary Globally, grasslands are both common and important landscapes, but less studies have investigated the influence of hillslope processes on these environments and their properties. This study investigated a coastal grassland on a hillslope at Point Reyes National Seashore, California, by combining data sets from different disciplines, covering satellite, field, and laboratory measurements. The site could be grouped into four environmental zones with different properties along the hillslope. Satellite measurements revealed that plants were more active in the wetter, down-slope throughout the dry summer months. Soil carbon content was not linked directly to soil moisture. Yet, soil carbon dioxide emissions were related to soil moisture, displaying three different behaviors depending on the moisture level. First, soil carbon dioxide emission was lower in the down-slope during the wet months (negative relationship), but then behaved similarly at all slope locations during the summer and early fall, and increased when it rained (positive relationship). The clustering analysis showed that our site varied significantly over a small distance (<8 m elevation and 150 m distance) and time (1 yr). Beyond the investigation of this specific site, this study highlights an approach for combining data sets to study ecosystems along hillslopes.

Key Points:

- The study used a critical-zone approach to combine multidisciplinary data sets and characterise a California coastal grassland
- Heterogeneity was large over a short distance (<150 m) and time (1 yr) and could be clustered by landscape position into four distinct zones
- Soil CO_2 fluxes exhibited contrasting responses to soil moisture, which differed with slope and season at the grassland

Supporting Information:

Supporting Information may be found in the online version of this article.

Correspondence to:

M. C. Rowley,
mike.rowley@geo.uzh.ch

Citation:

Rowley, M. C., Falco, N., Pegoraro, E., Dafflon, B., Gerlein-Safdi, C., Wu, Y., et al. (2024). The importance of accounting for landscape position when investigating grasslands: A multidisciplinary characterisation of a California coastal grassland. *Earth's Future*, *12*, e2023EF004208. https://doi.org/10.1029/2023EF004208

Received 30 NOV 2023
Accepted 13 MAY 2024

1. Introduction

Grasslands and the soils that support them are globally important ecosystems (Bai & Cotrufo, 2022; Dass et al., 2018). Grasslands cover approximately 40% of Earth's non-ice-covered terrestrial surface (e.g., excluding Antarctica and Greenland; Suttie et al., 2005) and their productivity is integral to the ecosystem services that they provide such as maintaining biodiversity, pollination, grazing, and cultural services (Bengtsson et al., 2019). Below the surface, grasslands are also critical for watershed yields, flood prevention, erosion control, and terrestrial carbon storage (Jankowska-Huflejt, 2006; McSherry & Ritchie, 2013). Grasslands store an estimated one third (31%) of global soil organic carbon (SOC) stocks in the top 1 m (Bai & Cotrufo, 2022; Bardgett

et al., 2021; White et al., 2000). Yet, the carbon stocks and vegetation species coverage in grasslands can vary significantly with topographic processes and across hillslopes, where there has been relatively less study (Ata Rezaei & Gilkes, 2005; Buraka et al., 2022; Harris et al., 2018; Lin et al., 2016; Singh & Benbi, 2018). It is critical to increase our understanding of how grasslands vary across hillslopes to better inform Earth System Models and management practices that seek to protect grasslands and their globally important ecosystem services.

More than 10% of California's land area is classified as grasslands, and more than 15% of the state's area is categorised as grazing lands, all covering terrain with complex topography (Eviner, 2016; Lin et al., 2016; Silver et al., 2010). Coastal grasslands (350 k ha) are important ecosystems (Jantz et al., 2007) that account for *ca*. 12% of all grasslands in California (3 M ha; Huenneke, 1989). Most coastal-grassland studies have focused on discrete points in a landscape or in locations with little relief (Bennie et al., 2008; Rowley et al., 2023; Zhao, 2022). However, topography plays a key role in driving pedogenesis and soil biogeochemical functioning, creating landscape units that have different environmental properties, such as distribution of vegetation, soil moisture, and SOC (Buraka et al., 2022; Fissore et al., 2017; Singh & Benbi, 2018). Lin et al. (2016) examined the relationship between land surface parameters and SOC stocks of a California grassland at Sedgwick Reserve, demonstrating that curvature and aspect could explain 50% of the variability in soil C stock. This highlights the importance of considering hillslopes when investigating the subsurface dynamics of California's coastal grasslands.

The critical zone is the region of the Earth's surface where vegetation, hydrology, and regolith (soils and saprolite) interact, and its spatio-temporal evolution is fundamental to the maintenance of the ecosystem services afforded by grasslands (Brantley et al., 2007). The critical-zone approach considers relief as an integral component of an ecosystem (Chorover et al., 2007; Council, 2001) and necessitates the combination of multidisciplinary data sets that typically span different temporal and analytical scales (Brantley et al., 2007; Rasmussen et al., 2011). For example, remotely sensed measurements (satellite imagery and spectral data) and geophysical methods (soil electrical conductivity) can provide rapid spatially- and temporally-resolved data on the evolution of the surface and subsurface, respectively (Dafflon et al., 2023; Dafflon et al., 2017; Falco et al., 2021; Rudolph et al., 2015; von Hebel et al., 2018). These measurements can then be constrained with direct point measurements of plant biomass and soil profiles or cores, which evaluate precisely the given properties of vegetation or regolith at one space and time (Rowley et al., 2020; Ryals et al., 2014), but are relatively time-consuming. To investigate how the environmental heterogeneity in these multidisciplinary data sets is distributed across space and time, a clustering technique can be used to identify distinct environmental zones that have unique distributions of ecosystem properties (Devadoss et al., 2020; Hermes et al., 2020; Hubbard et al., 2013; Wainwright et al., 2015, 2021). This approach was recently used by Wainwright et al. (2022) to demonstrate that hillslope metrics can capture the majority of landscape heterogeneity in critical-zone dynamics at the East River watershed, Colorado. To our knowledge, no study has yet combined these methods to investigate the coastal grasslands of California and how their environmental properties are influenced by landscape position; thereby hindering our ability to predict how these important ecosystems in complex terrain may respond to future change such as shifts in climate.

To address this gap, we investigated how landscape position influenced the environmental properties of a coastal grassland in California. Our objective was to identify the spatial and temporal variability of critical-zone properties at our site and the influence that landscape position had on these properties. To investigate surface dynamics, we combined remotely sensed observations, aboveground biomass-, and soil CO_2 flux-measurements along the hillslope. We investigated spatial and temporal variations in the subsurface by measuring soil temperature, moisture, ground-water table (GWT) depth, and completing geophysical surveys of the hillslope, which were then constrained by the characterisation of soil cores. We combined these multidisciplinary data sets, applying clustering techniques to the landscape, linear mixed modeling, and petrophysical modeling approaches. Based on previous studies of grasslands (Buraka et al., 2022; Harris et al., 2018; Singh & Benbi, 2018), we hypothesised that soil moisture would increase moving down the hillslope and drive shifts in vegetation (community and increasing biomass), SOC (increase), and soil CO_2 fluxes (decrease).

2. Methods

2.1. Site Setting

Point Reyes National Seashore is a nature reserve situated in a hilly environment, north of San Francisco. The region has a mean annual temperature of 11.7°C and annual precipitation of 750 mm, which predominantly falls between November and March. The grasslands of Point Reyes are dominated by perennial and annual grasses

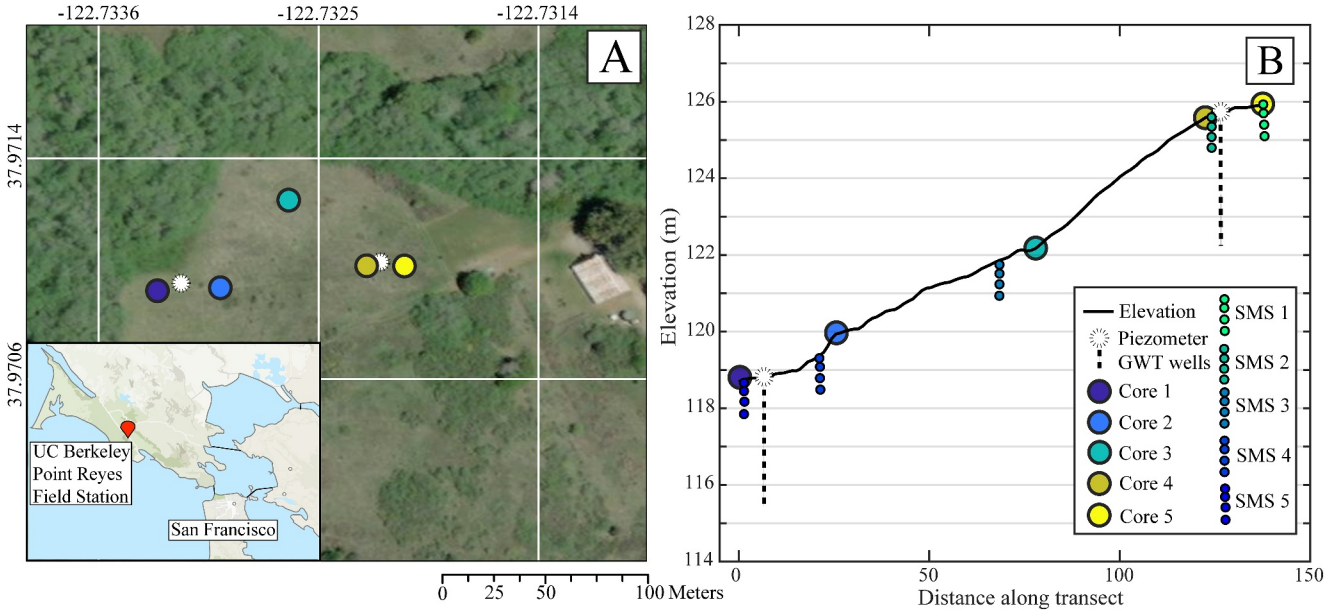

Figure 1. The Point Reyes Field Station (PRFS). (a) Soil core and piezometer well locations at the PRFS (See Figure S1a in Supporting Information S1 for other sensor locations). (b) Soil core, soil moisture sensors (SMS), and piezometer well locations and their relative depths along the PRFS hillslope. The *x* and *y* axes are not to scale and are plotted relative to the different axes.

such as *Danthonia californica*, *Festuca californica*, *Holcus lanatus*, *Stipa pulchra*, and *Poa Pratensis* (Amme, 2008). The Point Reyes Field Station (hereafter PRFS; 37.9708, −122.7309; Figure 1a) is a research unit within the National Seashore, which is delimited by the San Andreas fault in the east, Olema creek to the north, and Pine Gulch creek to the west. A brief history of anthropogenic activity at the PRFS can be found in Supporting Information S1. We evaluated how environmental properties varied over a small hillslope (<8 m elevation in 150 m; Figure 1b) at the PRFS, which had a 14% slope angle at maximum and a western aspect.

3. Above Ground Measurements

3.1. Weather Station Data

A weather station was installed at the site by the University of California Natural Reserve System in December 2019 (37.9697, −122.7317; https://dendra.science/orgs/ucnrs/status/point-reyes). A subset of this data is presented including temperature, precipitation, and percent time with conditions supporting fog or dew (quantified as time when atmospheric humidity ≥100% or air temperature < atmospheric dew point). Data is continuously recorded every 10 min, excluding data loss due to a memory card malfunction between 12 August and 4 October 2021.

3.2. Remote Sensing

We obtained four satellite multispectral PlanetScope Analytic Ortho images with a 3 m resolution, which were acquired on 25 September 2020, and 7 March, 27 April, and 31 May 2021. These dates were chosen to ensure that the characterisation sampling efforts and seasonal changes at our site closely matched the remotely sensed data. From the remotely sensed images, we computed the normalised difference vegetation index (NDVI) as described in Supporting Information S1. The NDVI was used to characterise the temporal and spatial variability in vegetation productivity (Devadoss et al., 2020; Wainwright et al., 2020). We used a 1 m resolution digital elevation model (DEM) produced through the 3D Elevation Program (3DEP) developed by U.S. Geological Survey to extract several topographical metrics, including elevation (Figure S1b in Supporting Information S1), slope (Figure S1c in Supporting Information S1), aspect, solar insolation, topographic position index, topographic wetness index, and curvature. The solar insolation was calculated for a specific location in a year of clear sky (W m^{-2} yr^{-1}) following the approach of Kumar et al. (1997).

3.3. Aboveground Vegetation Biomass

Aboveground vegetation was harvested at our sites at two separate intervals. Biomass was harvested at its largest height peak growing season (between 15–17 June 2021) in ten plots that measured 0.4 × 0.9 m each and spanned the hillslope (Figure S1a in Supporting Information S1). Vegetation was sorted by dead and live biomass, further sorting live biomass by individual species. Vegetation was dried at 45°C for >48 hr and weighed to obtain dry mass (g m^{-2}). A vegetation survey was completed by a Point Reyes National Seashore botanist (Shelly Benson), who specialises in the identification of California coastal grassland species. The botanist helped to constrain whether the species were annual or perennial, and their growth form (forb, grass-like, or grasses).

3.4. Soil CO_2 Flux

Soil CO_2 flux was measured during 2021 at three locations (Figure S1a in Supporting Information S1) along the transect using forced diffusion (FD) soil CO_2 flux sensors (Eosense, Canada). Measurements were made continuously in 30 min intervals. The FD sensors were placed into soil collars installed 5 cm into the mineral soil (7.5 cm inner diameter; 9.0 cm outer diameter; 5 cm height). The FD chambers were deployed on 23 November 2020 and here we report all available data ranging from February to November 2021. The downslope sensor malfunctioned for two periods in 2021, first in early April to late May, and again from late June to late August. Subsequent measurements (FD, Eosense) were made in 2022 at future whole-profile soil warming plots (24 sensors in total) placed throughout the different landscape positions, logged in 30 min intervals, and have been included in the SI to support our observations from 2021. In every warming plot, sensors were placed adjacent to *Holcus lanatus* to minimalize differences in soil CO_2 flux caused by a variation in grassland species.

4. Subsurface Measurements

4.1. Soil Sampling

Five soil cores were sampled along the hillslope at the PRFS (Figures 1a and 1b), between October and December 2020. All soils were historically grouped (Tomales series; NRCS, 2022; SoilWeb, 2021) and characterised using the World Reference Base system (IUSS Working Group WRB, 2015). Each core was sampled in 10 cm intervals to 100 cm where possible and transported to the Lawrence Berkeley National Laboratory for further analysis. Roots and large fragments (>2 mm) were separated for bulk density. A subsample of moist soil was dried at 105°C to calculate gravimetric water content. Soil subsamples used for chemical analyses (see below) were oven dried at 40°C and measurements were corrected for hygroscopic moisture content (van Reeuwijk, 2002). A subset of dried soil samples were ground with a Retsch MM400 ball mill for 48 hr at a frequency of 1,800 rpm^{-1}. Blind replicates and process blanks were measured throughout analyses to check analytical replicability and precision.

4.2. Soil Physico-Chemical Analysis

A suite of physico-chemical characterisation analyses was completed on all soil core samples. Soil pH was measured potentiometricly in 1M KCl (1:2.5 ratio) using a glass-body combination electrode (VWR 89231-574; Pansu & Gautheyrou, 2006). Similar measurements were made in distilled water to verify our measurements and were typically 1–1.5 pH units higher and less reproducible than the KCl measurements (data not shown), as previously reported (see Sumner, 1994 for detailed explanation). Soil CHN analysis was completed on ground samples using a Costech 010 Elemental Analyzer at the University Hawaii Hilo Analytical Lab. Soil particle size distributions were determined for each sample with laser diffraction using a Malvern Mastersizer 3000 and a Hydro LV module. Samples were pre-treated (see Supporting Information S1; Pansu & Gautheyrou, 2006) then loaded into the Hydro LV module with a pump speed of 3000 rpm^{-1} and sonicated (100%), prior to manually measuring samples in triplicate using the Fraunhofer optical model. Soil exchangeable cations were extracted using cobalt hexamine extractions (Aran et al., 2008), diluted in 2% HNO_3, combined with an internal standard, and then measured using a Perkin-Elmer Sciex Elan DRC II inductively coupled plasma mass spectrometer. The cation exchange capacity (CEC; $c.mol_{c.}\ kg^{-1}$) represents the sum of extracted cations (Al^{3+}, Ca^{2+}, Mg^{2+}, Na^{+}, K^{+}), not including H^{+}. Base saturations were high and not affected by the inclusion of H^{+} into CEC sum calculations, using soil pH to approximate its concentration.

4.3. Soil Total/Trace Element Concentrations and Mineralogy

Total element composition of our soil cores was measured at three depth intervals (*ca*. 0–10, 30–40, and 60–70 cm) following lithium tetraborate fusion of ground samples and the subsequent dissolution of the fused discs at ALS Global (ME-ICP06). 0.1 g of ground soil was added to a lithium metaborate/lithium tetraborate ($LiBO_2$/$Li_2B_4O_7$) mixture and furnaced at 1000°C. Discs were then dissolved in a weak acid (100 mL 4% HNO_3 and 2% HCl) and measured with inductively coupled plasma-atomic emission spectroscopy for whole rock elements (major) and inductively coupled plasma-mass spectrometry for trace elements. Results were corrected for mass loss-on-ignition. Various weathering indices were created by calculating ratios between mobile and immobile elements (see Supporting Information S1 for details; Schaetzl & Thompson, 2015). The mineral composition of ground soil core samples was ascertained semi-quantitatively at the same 3 depth intervals (*ca*. 0–10, 30–40, and 60–70 cm) using X-ray diffraction at the Stanford Synchrotron Radiation Lightsource (BL 11-3) with the methods outlined in Supporting Information of Rowley et al. (2023). The mineral composition of soil core 3 could not be measured due to beam time limitations.

4.4. Measurements of Soil Moisture and Ground-Water Table (GWT) Elevation

To investigate fluctuations in the GWT, two piezometer wells were installed, one at the top of the hillslope (37.9711, −122.7323) and another at the bottom (37.9710, −122.7331; Figure 1b). Both wells were *ca*. 3.5 m deep and equipped with pressure transducers (Onset U20). The elevation of the GWT was inferred by correcting the measured pressure with barometric pressure and real time kinematic global positioning system measurements. Measurements were made every 30 min for 1 yr between January 2021 and 2022. The GWT fell below measurement depth in the summer months, falling below the sensor between 27 July-24 October and 10-24 October at the top and bottom of the hillslope, respectively. The GWT readings were verified through manual measurements. Soil moisture and temperature sensors (TEROS 12, METER Inc) were also installed at four depths (10, 30, 60 and 90 cm depth) at five locations along the hillslope (Figure 1b & Figure S1a in Supporting Information S1). Installation was completed by auguring a 10 cm diameter hole, before inserting the sensors into the wall at the 4 depths, and then refilling the hole with excavated material. Soil moisture and temperature measurements were autonomously collected at 30 min intervals. Like soil CO_2 fluxes, soil moisture data for 2022 was also collected at the future whole-soil warming plots using EnviroSCAN probes (Sentek Tech., Australia) installed at 8 depths (10, 20, 30, 40, 60, 80, 100, and 120 cm) in a soil moisture probe system, logged at 30 min intervals, and presented in Supporting Information S1.

4.5. Geophysical Imaging

Geophysical methods, such as EM surveys, are frequently used for subsurface hydrological investigation as they can analyze large spatial scales, beyond point measurements, and enable the investigation of subsurface temporal dynamics (Hubbard & Rubin, 2005). An EM survey was completed to investigate fluctuations in soil electrical conductivity (EC) at the PRFS hillslope and assess subsurface spatial and temporal variations. The vertical and lateral distribution of soil EC across the study site (<200 cm depth) was quantified using a ground-based frequency-domain EM induction device. The EM survey was conducted by completing multiple transects across the field site, automatically recording the geographic coordinates with a real time kinematic global positioning system (Hyper V, from Topcon Inc). The EM induction device had six horizontally oriented coplanar coils with dipole center distances of 20, 33, 50, 72, 103, 150 cm (CMD Mini Explorer 6L from GF Instruments Inc.). The instrument was maintained at 10 cm above the soil surface throughout measurements.

In order to reconstruct the depth-discrete distribution of soil EC, EMagPy was used to invert the EMI data (McLachlan et al., 2021). The inversion process aims to minimize the difference between measured values and the values generated from forward model calculations. A non-linear full solution forward 1-D model was used to invert the data, based on Maxwell's equations (Frischnecht, 1987). The depth-discrete model was parameterised with nine layers with boundaries at 25, 50, 75, 100, 125, 150, 200, 250 cm depth. Finally, the inferred data were corrected to a temperature of 20°C by applying a fractional change in EC of 1.83%°C^{-1} (Hayley et al., 2007). The temperature offset from 20°C was estimated based on the depth-discrete monitoring of soil temperature at 10, 30, 60, and 90 cm depth at multiple locations (TEROS 12), which were here spatially averaged, and interpolated or extrapolated to each model layer depth.

The EM data was acquired on 24 September 2020, and 6 March, 28 April, and 28 May 2021. The acquisition on 24 September 2020, when the soil was relatively dry with little spatial variability in soil moisture, was intended to identify the impact of heterogeneity in soil texture and porosity on the measured signal. Data sets collected in 2021 were used to evaluate changes in soil moisture, and to correspond to the remotely sensed data. Controls on soil EC include clay content, grain surface conductance (primarily driven by clay content), soil cementation, porosity, EC of pore water, soil moisture, and temperature (Archie, 1942; Dafflon et al., 2013; Friedman, 2005). In environments where EC of the pore water does not vary extensively, the spatial variability in soil EC is primarily related to changes in moisture content (Dafflon et al., 2017; Falco et al., 2019) and/or soil properties (e.g., porosity, clay content; Falco et al., 2021). Such relationships are generally site specific and evaluated by verifying the EM data with co-located point measurements on soil samples. Following this approach, the EM data was used to extrapolate point measurements of soil properties (e.g., texture) to the site scale.

4.6. Statistical Analysis

To capture the aboveground and belowground spatial heterogeneity across the study area we combined several modeling techniques. We used a clustering approach to group landscape heterogeneity and to identify spatial zones with unique properties at our site. The feature set used for clustering analysis was composed of several data sets, including the time-series of soil EC at the depth of 62.5 and 87.5 cm, time-series of NDVI, and various topographical metrics, such as elevation, slope, aspect, potential total solar radiation, topographic position index, topographic wetness index, and curvature. To account for the different spatial resolutions of the data sets included in the clustering analysis, all data sets were transformed to the same spatial grid of the lowest resolution data set (3 m NDVI). The feature set was then standardised and reduced by applying principal component analysis (PCA). The final feature set was composed by the first few principal components representing 99% of the total variance. The adopted clustering algorithm uses an agglomerative hierarchical procedure, in which data points are merged within the same cluster using a similarity metric in a bottom-up approach (Ward's minimum variance criterion). We calculated the optimum number of clusters using a silhouette analysis (Pedregosa et al., 2011; Rousseeuw, 1987).

The effects of landscape position, profile, and horizon on soil properties were investigated using linear mixed models in SAS 9.4® (SAS Institute, Cary NC). To account for autocorrelation with depth, models included soil depth classes (10 cm intervals) as a repeated measures effect, blocked by profile, with a first-order autoregressive covariance structure (selected by Bayesian Information Criteria). Model residuals were checked for normality using QQ-plots and were plotted against predicted values to evaluate goodness of fit and any deviations from homoscedasticity (Galecki & Burzykowski, 2015). The significance of fixed effects were evaluated using type III F-tests, while the denominators' degrees of freedom were computed using the Satterthwaite adjustment (Satterthwaite, 1946). The means of significant fixed effects were compared using t-tests without multiple inference adjustment. The reported means are conditional least-square means ± the standard error of the mean, the alpha level of which was set to $\alpha = 0.05$. A PCA was also run on the correlation matrix of our soil analyses (CEC, pH, CHN, clay content) to synthesise relationships between soil properties and to explore the co-variability in our data sets.

5. Results

5.1. Weather Data

Daily temperatures ranged from 4.4 to 14.9°C during the winter months and between 11.1 and 19.4°C during the summer months in 2021 (Figure 2a). Data outside 2021 is presented in Supporting Information S1 (Figures S2a and S2f). All precipitation fell as rain, with 99% (in 2021) of rain falling between October (starting 19 October) and March (hereafter the wet season), while April through September received virtually no rain (hereafter the dry season; Figure 2b). Wind direction was predominantly NW-SE in 2021, aligned with the direction of the Olema Valley (Figure S3 in Supporting Information S1). The months with the highest average percent time with conditions supporting fog or dew (i.e., percent of time when no active rainfall was occurring, but relative humidity was 100% [fog] or air temperature was below the air dew point [dew]) were November, December, and January. However, July and August also had comparable averages (Figures S2e and S2f in Supporting Information S1), due to water inputs from fog and dew during the summer months of July and August. While seasonal weather

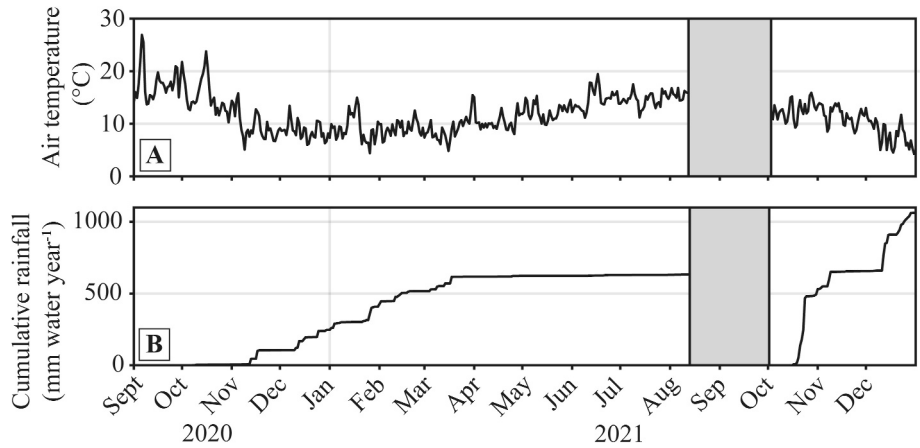

Figure 2. Meteorological data from the Point Reyes Field Station recorded between September 2020 and December 2021 (see Figure S2 in Supporting Information S1 for data outside of this range). (a) Daily average air temperature (°C), the shaded gray box represents a period of data loss due to a memory card malfunction. (b) Cumulative water year rainfall (mm; starting 1 October 2020 or 2021).

patterns were consistent across our sampling site, there was significant spatial variation in critical-zone properties depending on landscape position.

5.2. Identification of Environmental Zones

Critical-zone properties were grouped into four distinct zones at the PRFS by a clustering algorithm (Figure 3). The clustering delineated zones of three regions of roughly equal size that were distributed east to west across the site and were split by topographic gradient, with a smaller fourth region bordering the riparian transition to the north- and south-western edge of the PRFS. Zones 1–3 transitioned down the hillslope. The zones will hereafter be referred to as the up-slope (Zone 1), mid-slope (Zone 2), down-slope (Zone 3), and the bordering riparian ecotone (Zone 4). The high-water table in this fourth zone (Figure 3), which bordered the Olema creek to the north and Pine Gulch creek to the west, was atypical of the coastal grasslands of California, and was more representative of an ecotone to the surrounding riparian zone. Our results and interpretations are focused on the up- to down-slope area of our hillslope (Zones 1–3).

5.3. Subsurface Hydrology

After the wet season, the GWT elevation at both wells slowly fell from <1 m at the end of March to >4 m below the surface in early October. The GWT was closer to the surface and fell more slowly between March and August in the down-slope. The difference in GWT depth at the up- and down-slope was typically 0.8 m (mean = 0.8 m, median = 0.6 m, minimum = 0.3 m, n = 10,179), but increased after rainfall events (≤2.25 m) and during the dry months, where the up-slope GWT fell first (up to 1–1.5 m; Figure S4b in Supporting Information S1). The groundwater table (GWT) elevation increased by *ca*. 3 m in both up-slope and down-slope areas during the first major rainfall event of the water year (Oct.), increasing from >3.4 m below the surface at both wells to 0.5 (up-slope) and 0.2 m (down-slope) below the surface (Figure 4a and Figure S4a in Supporting Information S1). We note that GWT elevation right before this rainfall event is not known precisely (as it occurs deeper than the pressure transducers). Overall, there was a lag of approximately 2 days between when the GWT was first registered down-slope (04:30, 22.10.21) and up-slope (00:30, 24.10.21). After the start of the rainfall event, the rising GWT reached 2 m depth in less than 3 and 5 days at the bottom and top of the hillslope, respectively.

Soil moisture decreased with increasing soil temperature (Figure S5b in Supporting Information S1), decreasing gradually into the dry season, first in the surface horizons and then deeper depths (Figure 4b). There was a large increase in soil volumetric moisture within 2 days after the start of the first major rainfall event (Figures 4a and 4b). Soil moisture rapidly increased, first in the down-slope (11:30, 20.10.21) and then the up-slope (23:45, 20.10.21) after the first major rain event (18:30, 19.10.21) of the water year (>4 mm, there was also a small rain pulse 17.10.21), approaching saturation (*ca*. 0.4 vol/vol). The moisture content of the soils also varied between

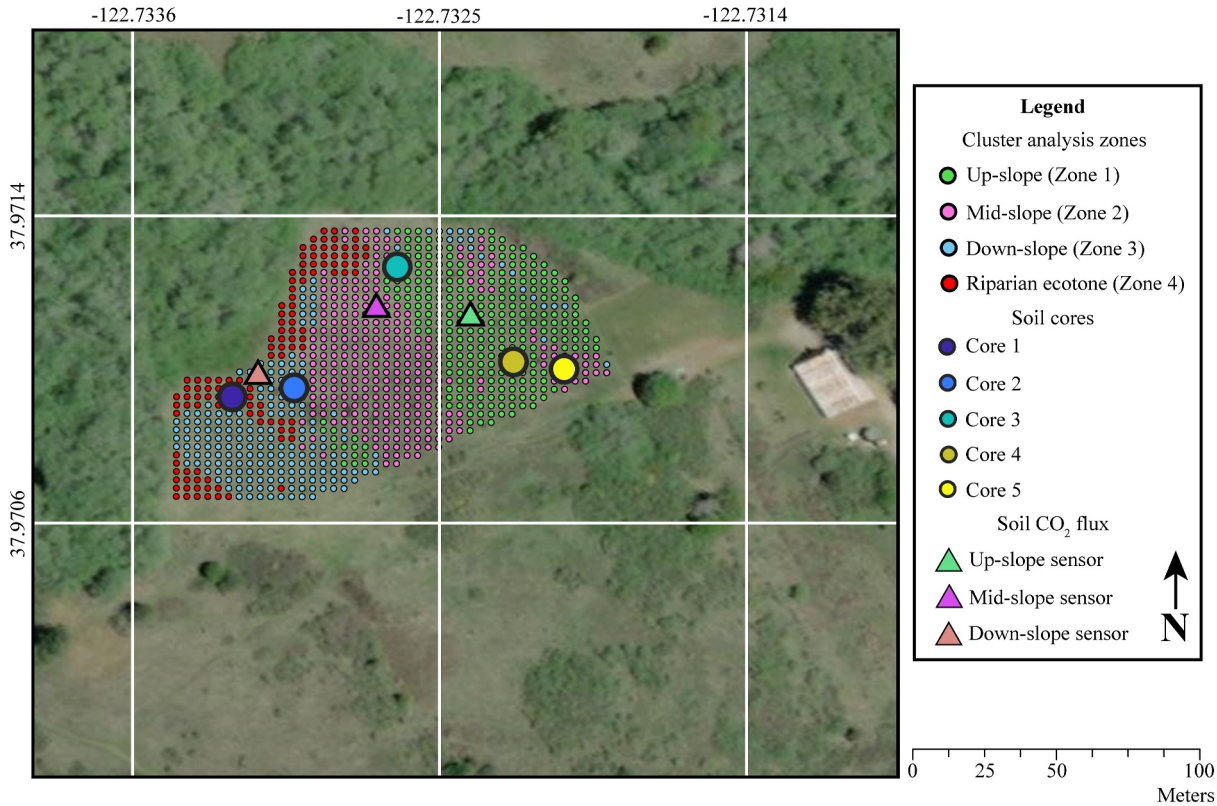

Figure 3. Clustering analysis results from the Point Reyes Field Station (PRFS) revealed that the site could be broadly split into four distinct zones, an up-slope (Zone 1), mid-slope (Zone 2), and down-slope (Zone 3), with a final riparian ecotone region (Zone 4) bounded around the north- and south-western edge of the PRFS.

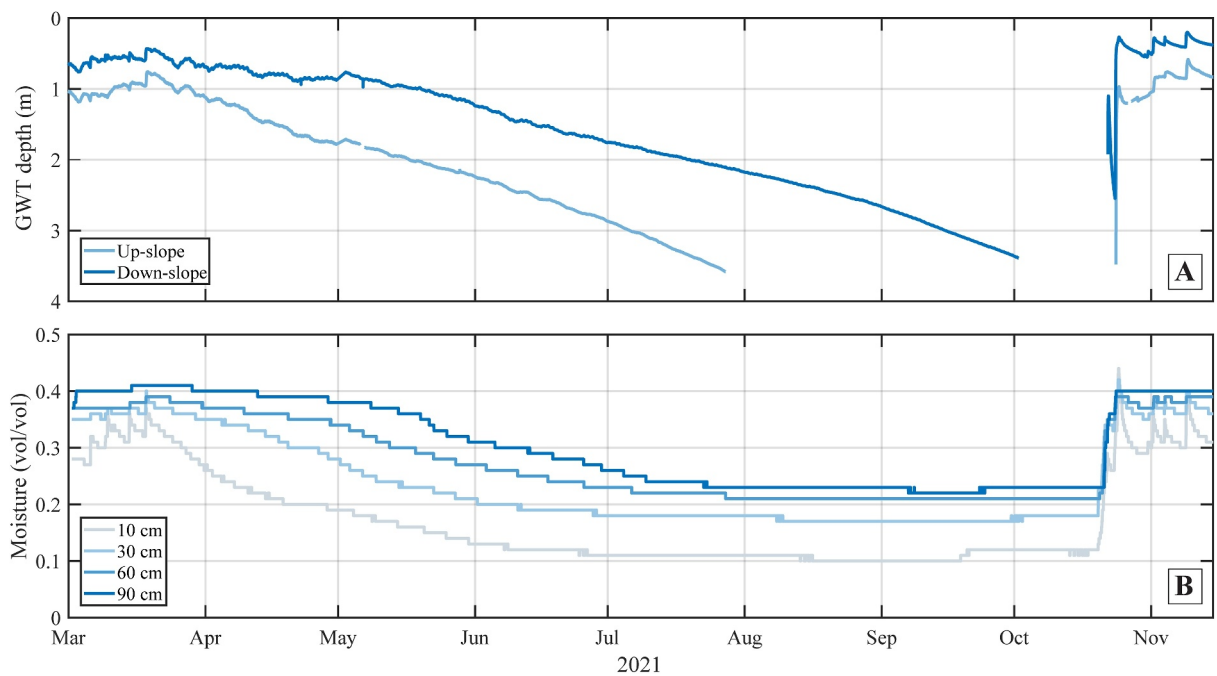

Figure 4. (a). Groundwater (GWT) table elevation at the up-slope (dark blue) and down-slope (light blue) wells between March and November 2021, when we have soil moisture measurements also (see Figure S4 in Supporting Information S1 for all GWT data in 2021 and difference between sensors). (b) Average soil moisture content at four depths from the five soil moisture sensors located across the Point Reyes Field Station (see Figures S5 and S7 in Supporting Information S1); the colors indicate sensor depth as defined in the legend, while soil moisture content is measured as a decimal fraction (0%–50%).

10.1029/2023EF004208

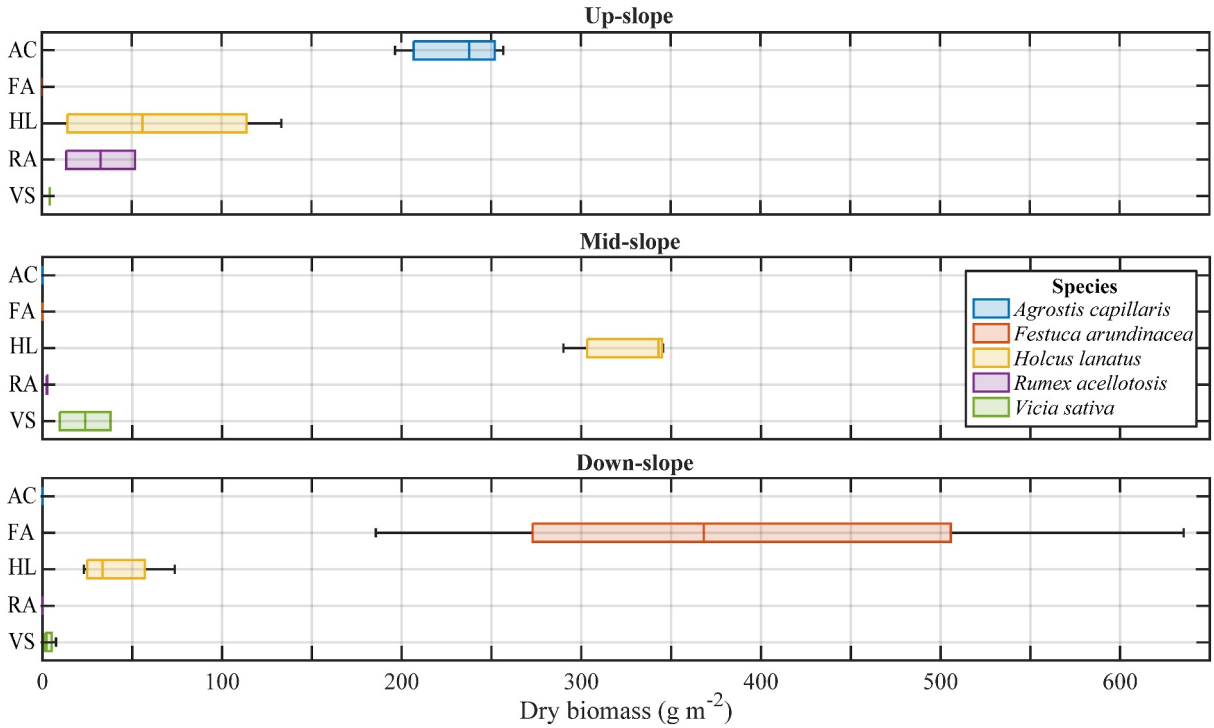

Figure 5. The distribution and abundance of grassland species (dry biomass g per m^{-2}) from the ten cultivation sites (Figure S1a in Supporting Information S1) split by cluster analysis identified zones.

the up-, mid-, and down-slope (Figures S5c and S6 in Supporting Information S1), staying wettest for the longest in the down-slope and decreasing first in the mid-slope (Figure S7 in Supporting Information S1), which had the highest slope angle.

5.4. Aboveground Biomass by Landscape Position

Vegetation species and aboveground biomass varied with landscape position. Table S1 in Supporting Information S1 lists all the species identified in ten quadrat locations that were harvested for aboveground biomass measurements, detailing whether the species are native, perennial or annual, and their growth form. The coastal grassland at PRFS was dominated by non-native, perennial grasses. Overall, *Holcus lanatus* was the most abundant species at our site, but community composition, relative abundance (in cover), and dominant vegetation classification changed with landscape position (Figure 5). There was also a small variation from south to north, but this was to a lesser extent. In the up-slope, *Agrostis capillaris* dominated (>30% relative cover) or co-dominated with *H. lanatus*. Mid-slope, *H. lanatus* was the dominant species, while in the down-slope, *Festuca arundinacea* dominated (Figure 5). Aboveground biomass (dry g m^{-2}) also varied across the site (Figure S8 in Supporting Information S1); total biomass (up-slope = 1,045.7 ± 72.1 g m^{-2}, mid-slope = 1,264.7 ± 104 g m^{-2}, down-slope = 1,545.4 ± 225 g m^{-2}), like moisture, increased moving down slope due to an increased quantity of dead plant material (up-slope = 596.5 ± 71.2 g m^{-2}, mid-slope = 803.4 ± 65.3 g m^{-2}, down-slope = 1,076.7 ± 143.8 g m^{-2}), while live biomass did not vary significantly.

5.5. Remote Sensing of Vegetation

As expected, remotely sensed NDVI was lowest at the end of the dry season, September 2020, and increased towards peak growing season (May 2021; Figure 6). The NDVI scores displayed an overall trend towards increasing values moving down slope, increasing with moisture content and aboveground biomass (Figures S6a and S6c in Supporting Information S1). The differences between the up- and down-slope were largest in the dry season, before converging in the wet season (Figure S9 in Supporting Information S1). Inferred inbound solar insolation (Figures S6 and S10 in Supporting Information S1) was not strongly correlated with average NDVI as it was higher in the south of the mid-slope.

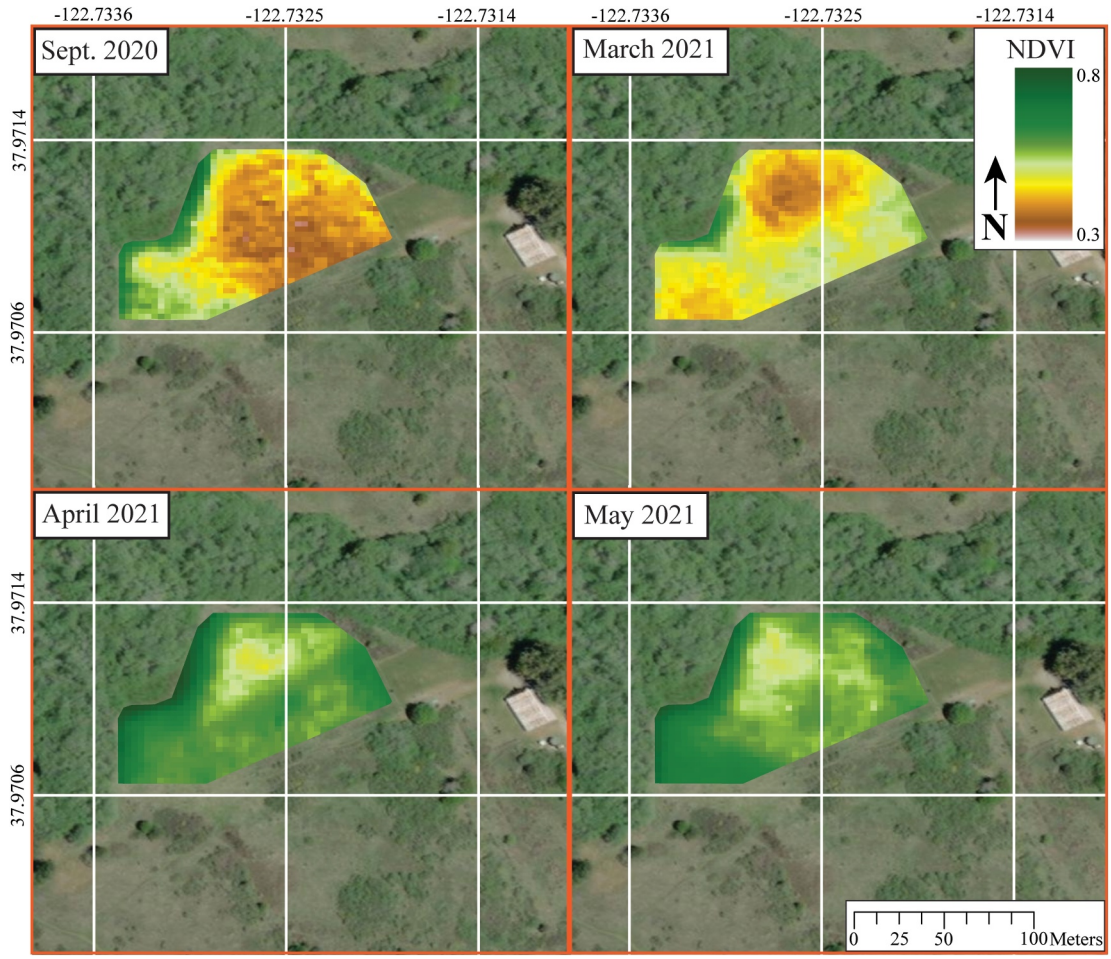

Figure 6. Normalised difference vegetation index (NDVI) values for the Point Reyes Field Station calculated from multispectral PlanetScope Analytic Ortho images with a 3 m resolution, acquired on 25 September 2020, and 7 March, 27 April, and 31 May 2021.

5.6. Soil Properties

The soils at PRFS were characterised as having an argic horizon (except Core 3) and were classified as a Ferric Luvisol (Core 1), Ferric Lixisols (Cores 2, 4, and 5), or a Eutric Cambisol (clayic; Core 3). The bulk soil properties of soil cores are listed in Figures 7a–7d and Table S2 in Supporting Information S1.

The bulk mineral composition of the soil cores in all locations was dominated by quartz and phyllosilicates, with small amounts of feldspars, feldspathoids, inosilicates (data except core 3 in Table S3 in Supporting Information S1). Total element concentrations for three depths from each soil core are presented in Table S4 and the trace elements in Table S5 in Supporting Information S1. Total Al tended to increase with depth, while total P and K tended to decrease with depth. Weathering indices such as the chemical proxy of alteration suggested that nearly all samples were "highly weathered," except for samples Core 1 samples 30–40 and 60–70 cm which bordered on "extremely weathered' (Table S6 in Supporting Information S1). The content of Na_{Exch}, Mg_{Exch}, and Ca_{Exch} increased down the hillslope and with depth, while the content of Al_{Exch} increased in all cores between A and B horizons, but not deeper. Soil pH (1 M KCl) was very acidic and ranged between 3.3 and 4.4 (Figure S11a in Supporting Information S1). Extractable Al increased as soil pH decreased into the argic horizon (Figure S11a in Supporting Information S1) and soil pH showed a negative exponential relationship with extractable Al content (Figure S11d in Supporting Information S1).

Soil texture shifted from sandy loam to silty clay with increasing depth, towards the northwest of the site, and down the hillslope (Figure 7c). Overall, there was a large decrease in sand content with depth from the A (40.2 ± 9.8%) to the C horizon (17.4 ± 9.8%), while silt (A = 39 ± 5.3% and C = 54.9 ± 5.3%) and clay content

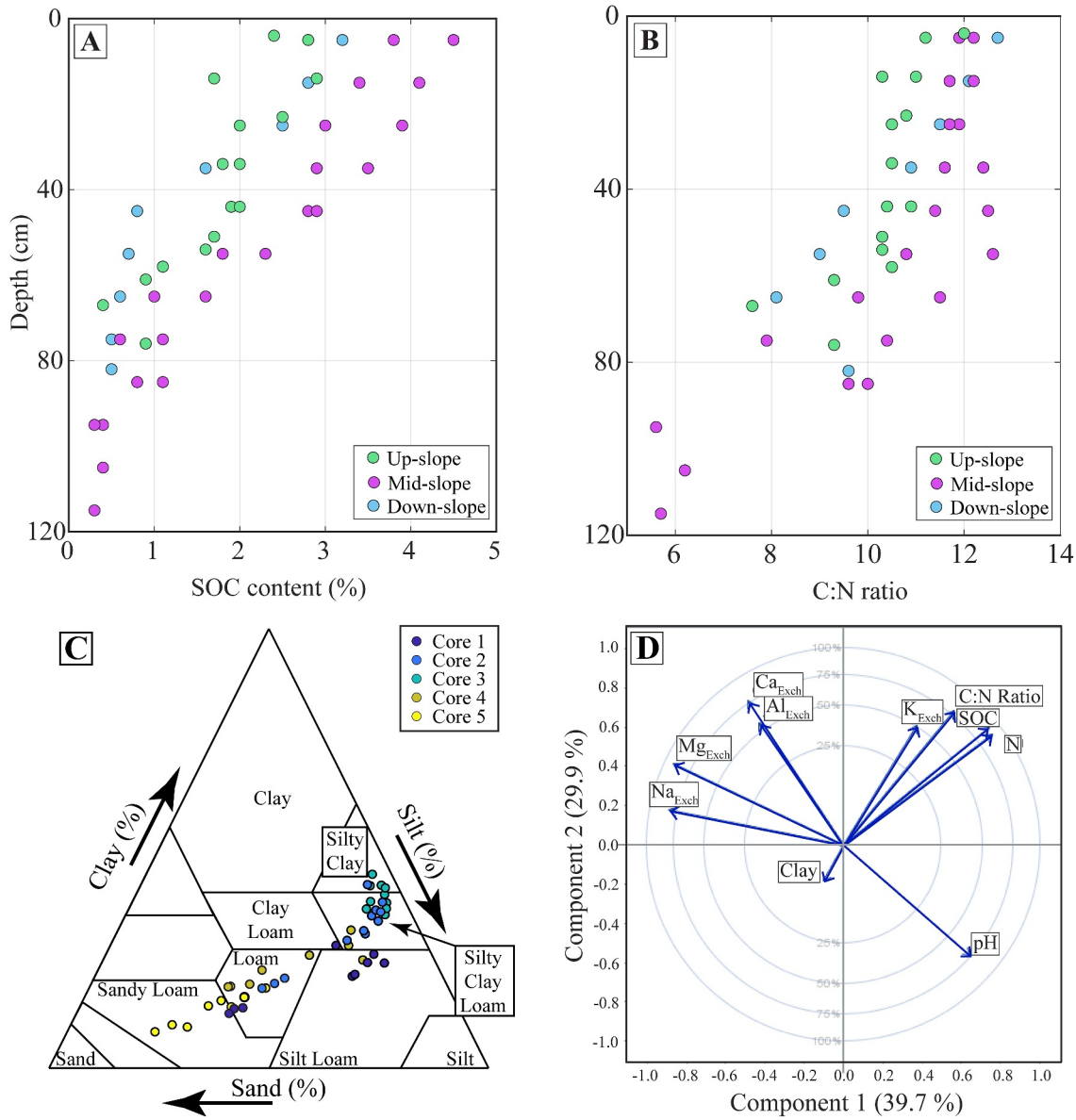

Figure 7. Soil properties of the soil core samples from the Point Reyes Field Station. (a) Soil organic carbon content (%) and (b) Carbon to nitrogen ratio split by landscape position. (c) Soil texture presented by individual core. (d) The results of a principal component analysis of soil variables of the PRFS soil core samples.

increased (A = 20.9 ± 4.4% and C = 27.8 ± 4.4%). As such, particle size distributions for the five soil cores showed an increase in smaller particle sizes with depth, as the fine sand content decreased, and the clay and fine silt fractions increased (Figure S12 in Supporting Information S1). Core 3 in the mid-slope maintained a high clay content throughout, and thus its particle size distribution evolved differently with depth relative to the other soil cores (Figure S12; Table S2 in Supporting Information S1).

Soil organic carbon (SOC) content varied with depth and landscape position (Figure 7a). Content of SOC decreased from 4.5% at the surface to 0.4% at 90 cm. Contrary to our initial hypothesis, SOC content was highest overall in the mid-slope. The down-slope had higher SOC content than the up-slope in the A horizon, but less in the subsoil horizons. The C:N ratio decreased with depth below 60 cm (Figure 7b), but SOC content and total N content remained largely collinear (Figure S11f in Supporting Information S1). The soil C:N ratios also displayed a similar pattern across landscape positions but was slightly higher in the A horizon samples of the down-slope.

Principal component analysis of different soil properties (exchangeable elements, C:N ratio, SOC, N, and clay content) revealed that variables that were related to the composition of soil organic matter (SOC content, C:N ratio, Total N) were largely unrelated to other geochemical variables (Figure 7d). The content of K_{Exch} was largely collinear with SOC content as it decreased with depth and displayed a biogenic profile. Soil pH was negatively correlated with most of the exchangeable elements, while clay content (increased with depth) was negatively correlated with the SOC content (decreased with depth). Similarly, neither peak NDVI or soil moisture were linked to SOC content.

5.7. Geophysical Surveys

The EMI-inferred soil electrical conductivity (EC) was higher in the wet season and then decreased into the dry season (Figure S13 in Supporting Information S1). Overall, soil EC trended towards higher values moving from the mid-slope to the riparian zone, but the up-slope maintained high soil EC values and was largely independent of the relationship moving down slope. The spatial and temporal fluctuations in soil EC could be linked to changes in soil moisture and soil properties. The relationship between soil EC and soil moisture measurements was time-dependent and was strongest during the wet season. In addition, soil EC responded differently to increased soil moisture based on its soil clay and silt content. Second-order polynomial regressions linking soil EC and soil moisture at various times indicated that the EMI-inferred soil moisture standard deviations were 0.04, 0.04, 0.055, and 0.041 vol/vol for 24 September, and 6 March, 28 April, and 28 May, respectively (Figure S14 in Supporting Information S1). The relationship strength was deemed insufficient to extrapolate soil moisture-based estimates across the site and indicated that soil moisture is not the main control on the spatial variability observed in the EMI data.

A bivariate analysis between soil EC and soil texture indicated that EC had the strongest positive correlation with clay and silt density in September 2020 ($R^2 = 0.53$; Figure 8a), when the soils were driest, although an up-slope soil core (5) location that was associated with a sandier texture in surficial horizons deviated from this relationship slightly. The correlation between soil EC, and clay and silt density were considered sufficient to estimate the spatial distribution of clay and silt density across the site and core 5 was included in this correlation (where EMI data were collected; Figures 8b and 8c). The residual standard deviation of inferred clay and silt density was 0.3 g cm^{-3}. Overall, the geophysical surveys, integrated with soil texture measurements, enabled us to extrapolate our point measurements and assess spatial variation in clay and silt density across the site. The specific relationship is field-site specific and was inferred when soil moisture was relatively low and homogeneous, but the approach should be generalisable.

5.8. Soil CO_2 Flux

Measurements of soil CO_2 flux were made continuously in the three hillslope zones (up-, mid-, and down-slope) in 2021 (Figure 9 and Figure S15 in Supporting Information S1). Soil CO_2 flux varied both spatially and temporally (Figure 9). As hypothesised, when soil moisture was the highest in the late winter and spring, daily soil CO_2 flux was lowest in the down-slope and highest in the up-slope. As the growing season progressed, soil CO_2 flux increased with NDVI and converged across all slope locations into the summer months. While there was one sensor per zone in 2021, in January-August 2022 sensors were deployed in 24 locations (Figures S16, S17, and S18 in Supporting Information S1), and similar patterns were observed.

In the dry months of 2021, as NDVI and soil moisture decreased, soil CO_2 flux rates dropped and averaged about 1 μmol m^{-2} s^{-1} across all landscape positions on the PRFS hillslope. After converging in the summer months, soil CO_2 flux rates increased rapidly and briefly after small rainfall events, exhibiting rain-pulse behavior, with notable examples 12-14 June and 22–25 June 2021. For the September soil CO_2 flux pulse, the PRNS meteorological station was not operational (Figure 2) but light rain was detected at a nearby weather station (2 mm rainfall 18 Sept.) and a small increase in soil moisture was detected at 10 and 90 cm (Figure S7 in Supporting Information S1). In addition to the rain pulses, soil CO_2 fluxes were also highly responsive to spatial patterns in soil moisture. As the new water year began, soil CO_2 flux among the zones diverged once again and were lowest in the down-slope. Data from a larger number of sensors in 2022 again demonstrated a strong link between soil moisture, as it varied by hillslope location, and soil CO_2 fluxes (Figure S17 in Supporting Information S1). In this wetter year (in which the average annual precipitation fell in just 1 month; Figure 2), soil CO_2 fluxes converged across all landscape positions instead in the wetter months, likely due to the near-saturated soil moisture

10.1029/2023EF004208

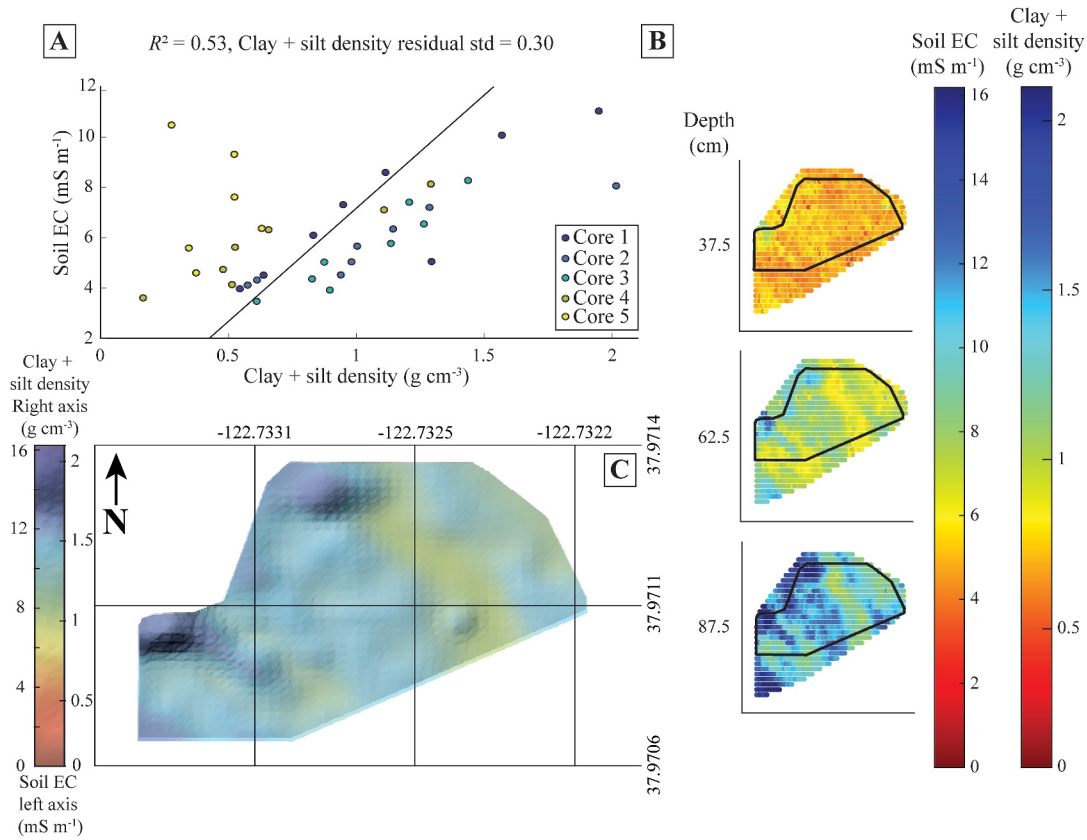

Figure 8. Geophysical survey results from the Point Reyes Field Station. (a) Positive relationship between co-located clay and silt density and soil EC data. The residual standard deviation between measured and estimated clay and silt density is equal to 0.3 g cm^{-3}. (b) Soil EC and inferred clay and silt density at different depth intervals in September 2020. (c) Soil EC and inferred clay and silt density at 62.5 cm, interpolated, with a Hill Shade effect, and cropped similarly to Figures 3 and 6.

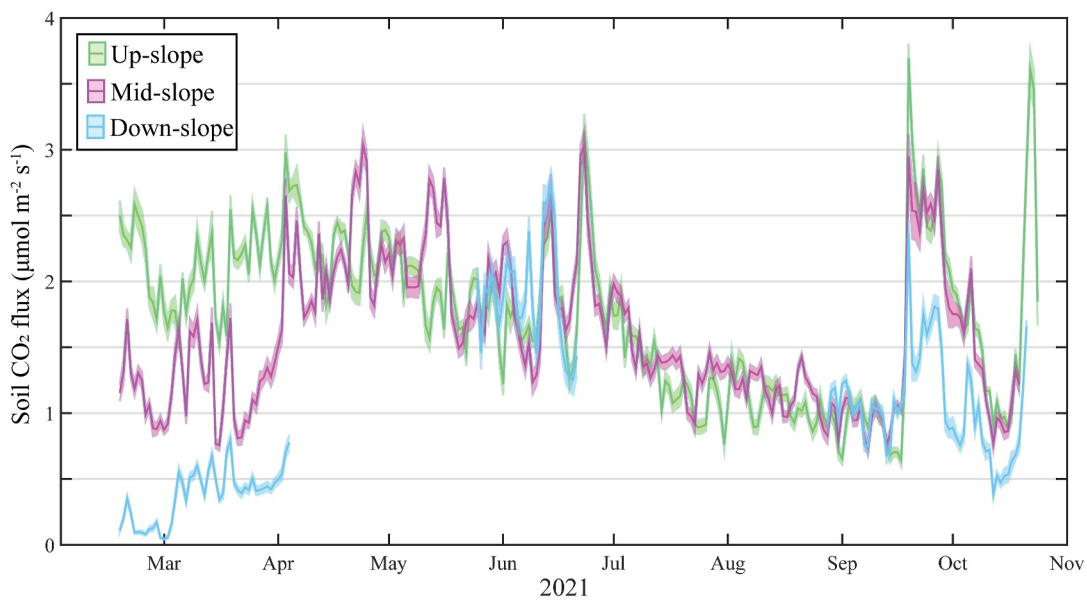

Figure 9. Daily average soil CO_2 flux (µmol m^{-2} s^{-1}) with the standard error of daily measurements reported as an error bar surrounding the daily mean. Data is only presented for the down-slope sensor when it was fully functional. All available data is presented in Figure S15 in Supporting Information S1.

conditions; while soil moisture remained higher in the dry season of 2022 than in 2021 and soil CO_2 fluxes were higher in the wetter downslope throughout the summer.

6. Discussion

6.1. Groundwater Fluctuations and Changes in Soil Moisture

California coastal grasslands are typically hilly environments (Lin et al., 2016; Stromberg et al., 2001) where subsurface hydrology can play an important role in the evolution of their critical-zone properties. An integrated view of both above- and below-ground processes, such as the critical-zone approach, is thus essential for investigating these environments (Huggett, 1975; Thompson et al., 1998). The critical-zone approach employed here highlighted the importance of considering landscape position when evaluating subsurface hydrological dynamics. Soil moisture decreased in the mid-slope (Figure S7 in Supporting Information S1) where slope angle was highest (Figure S1c in Supporting Information S1), approximately 0.5–1.5 months before it did in other landscape positions. The down-slope, on the other hand, stayed wettest for the longest period after the wet season, presumably driven by recharge of water from other parts of the watershed (Novák & Hlaváčiková, 2019).

The GWT elevation rose significantly at our site in the PRFS (>3 m). With our data set we cannot disentangle the controls on local and regional lateral flow versus vertical infiltration and believe that several different processes impacted GWT dynamics. The decrease in water-storage capacity with depth can participate in the significant rise in GWT elevation; quantifying vertical recharge, however, would require depth-resolved estimates of hydraulic conductivity of unsaturated soil (Carrera-Hernández et al., 2012). The rapid rise in GWT elevation is likely also driven by the surrounding hilly environment funneling surface and subsurface water towards the riparian region of the adjacent creeks to the north and west. Additionally, the complex subsurface hydrological pathways created by the tectonic activity of the nearby San Andreas fault and textural gradients could lead to preferential flow paths and accumulation of ground water in our study area (Bense et al., 2013; Galloway, 1977). A perched water table was found in certain locations of the site during drilling, which confirmed the complex nature of subsurface hydrological connectivity at our site. Overall, our site displayed significant heterogeneity in ground-water table and soil-moisture dynamics over a small hillslope (<8 m elevation difference); this highlights the importance of considering hillslope and subsurface structure when investigating the critical zone or ecosystems such as a grassland over complex terrain.

6.2. Vegetation and Biodiversity

By accounting for landscape position at our site, we identified important spatial heterogeneities in grassland species distribution with elevation (Figure 5), even over a small distance (*ca*. 150 m). The PRFS is dominated by non-native grassland species such as *Holcus lanatus* (Europe), *Agrostis capillaris* (North Africa, Europe, and central Asia), and *Festuca arundinacea* (Europe), which is similar to many other California grasslands, especially in mesic environments (Eviner, 2016; Stromberg et al., 2007). The ecological colonisation of California's grasslands by non-native species is thought to have been largely driven by drought and grazing (D'antonio et al., 2007; Eviner, 2016). The PRFS contains areas that were used as a cattle ranch before the National Park was incorporated (see Supporting Information S1 for more details; Livingston, 1995), which could have driven the installation of these species throughout the site. Yet, the current distribution of species is consistent with the observed soil moisture regimes (Figure 4 and Figure S7 in Supporting Information S1) and availability of water (Chambers et al., 2019; D'antonio et al., 2007; Nolan, 2021), which also had a strong impact on seasonal NDVI (health and vegetation density). Biomass amount indeed increased moving down slope with NDVI, which was due in part to the presence of tussock forming species (*Festuca arundinacea*), but also likely linked to the increased moisture availability in the dry season (Liu et al., 2021). Thus, as hypothesised landscape position had a cascading influence on vegetation community, its productivity, and biomass, due to its influence on water availability, ensuring that grassland vegetation dynamics were heterogeneous over a small spatial scale (Figure 5).

6.3. Pedology and Translocation

The soils on the hillslope also displayed significant heterogeneity over a short distance, varying with landscape position. Soils at PRFS were formed in highly weathered sedimentary rocks (Santa Cruz Mudstone and Santa Margarita Sandstone) formed in the Upper Miocene (Table S6 in Supporting Information S1; Clark & Brabb, 1997; Galloway, 1977). The finer material released from the sedimentary parent materials has translocated

and accumulated at different locations in our site with clay and silt density increasing with depth and towards the north-west of the site (Figure 7c and Figure S12 in Supporting Information S1). These shifts in texture were most likely driven by illuviation within profile and translocation of finer textured mineral particles down slope with the migration of moisture (Paton et al., 1995; Phillips, 2007). Exchangeable cations also demonstrated translocation (lixiviation), increasing in concentration into the illuviated horizons (Table S2 in Supporting Information S1). A notable exception was K_{Exch}, which displayed a biogenic concentration profile (Figure 7d; Brantley et al., 2007), possibly driven by historic nutrient application; but more likely, the active acquisition and cycling of K in the critical zone by vegetation, probably explaining the correlation between SOC and K_{Exch} (Hawkesford et al., 2012; Likens et al., 1994). Meanwhile the negative relationship between Al_{Exch} could indicate a role of gibbsite in buffering soil pH and dictating the depth distribution of pH in our acidic soils (Chadwick & Chorover, 2001; Slessarev et al., 2016). Overall, the soils at the PRFS displayed a significant degree of translocation, and thus, heterogeneity depended on both depth and landscape position, which could again be linked to the migration of water across our site.

6.4. Soil CO_2 Fluxes and Site Heterogeneity

Based on data from single continuous measurement systems located in the up, mid-, and down-slope, soil CO_2 fluxes differed spatially with landscape position on the hillslope and temporally with season in 2021. Soil CO_2 fluxes represent the combined respiration of roots, soil fauna, and microbes (Bowden et al., 1993; Wang et al., 2010) and were strongly linked to shifting soil moisture contents (Sanderman & Amundson, 2008, 2010). Low moisture conditions are commonly linked to decreased soil CO_2 flux rates in the grasslands of California (Fierer et al., 2005; Sanderman & Amundson, 2010) as water is a necessary component of decomposition and can influence root respiration. In these dry grassland environments, it is well established that soil rewetting during rainfall can lead to carbon turnover and substantial microbial respiration (Barnard et al., 2020; Birch, 1958; Placella et al., 2012). The principal driver of soil CO_2 rain-pulse behavior, or the Birch effect (Birch, 1958) in the grasslands of California is thought to be the substrate supply mechanism, particularly in the subsoil (Schimel et al., 2011; Xiang et al., 2008). This is because incubation studies and field experiments that manipulate drying and rewetting cycles in samples from the grassland soils of California have demonstrated that rewetting remobilises old C, leading to a pulse in microbial respiration (Schimel et al., 2011; Xiang et al., 2008). This mechanism is consistent with our observations during the dry months where soil CO_2 fluxes increased rapidly during small precipitation events in June or September 2021. However, the spatial pattern of soil CO_2 fluxes was not a simple function of increasing moisture content as seen previously in California (i.e., higher CO_2 fluxes with higher soil moisture).

Over 2021, we found that soil moisture seemed to instigate two distinct and contrasting responses on soil CO_2 fluxes. Similar to previous studies on the dry grasslands of California (Fierer et al., 2005; Sanderman & Amundson, 2010), we found that increases in soil moisture during the dry season caused pulses of increased soil CO_2 fluxes across all landscape positions (Schimel et al., 2011; Xiang et al., 2008). Yet as a second response not observed in these previous studies, increased soil moisture contents in the wet season were linked to lower soil CO_2 fluxes, particularly in the wetter down-slope. Water saturation can inhibit aerobic decomposition and its associated microbial respiration of CO_2 by limiting O_2 availability (Keiluweit et al., 2017; Schmidt et al., 2011; Skopp et al., 1990). The inhibition of respiration is plausible, especially as the downhill site at PRFS was far wetter, approaching saturation at shallow depths in the wet season which could have promoted anaerobic conditions and reduced soil CO_2 fluxes. Once the GWT elevation and soil moisture decreased at our site in the dry season in 2021, soil CO_2 fluxes increased and converged at the different landscape positions on the PRFS hillslope (oxygen limitation removed).

Subsequent soil CO_2 fluxes measurements in 2022 at the future whole-soil warming experimental plots (pre-warming; Figures S16, S17, and S18 in Supporting Information S1) supported observations from 2021, again demonstrating a strong control of soil moisture on soil respiration at the PRFS. In the 2022 data, soil CO_2 flux was again inhibited across the landscape positions by high soil moisture contents and were again lower in the mid- and down-slope. Yet, with the wetter conditions in the spring (significant rain events in late Mar., Apr., and June) soil CO_2 fluxes remained higher in the downslope site (Figure S17 in Supporting Information S1). This implies that in 2022 water-availability limitations did not inhibit soil CO_2 fluxes in the down-slope during the dry season (wetter than 2021). Overall, we propose that soil moisture instigated a dual threshold response in soil CO_2 fluxes; whereby, it either reconnected the microbial community to SOC substrates during rainfall events in the dry season

(removing water limitations) or inhibited aerobic microbial activity in the wet season (oxygen limitation), depending on landscape position and year at the PRFS. Future studies will now further investigate the interaction between soil CO_2 fluxes, soil moisture content, and future warming at the PRFS.

6.5. Soil Organic Carbon Content an Integrated Signal

We incorrectly hypothesised that SOC content would be higher in the down-slope at the PRFS due to its higher moisture content (Figure 4 and S7 in Supporting Information S1), but SOC was instead higher in the mid-slope (Figure 7a). While there was a weak positive relationship between bulk SOC and Ca_{Exch}, this relationship was far weaker than had been observed in soil cores taken from across Point Reyes with a larger soil pH range (Rowley et al., 2023). This was probably explained by the more acidic conditions at the PRFS (Figure S11A and Table S2 in Supporting Information S1), relative to the soil cores of Rowley et al. (2023), which would have increased competition between Ca_{Exch} and positively charged minerals or acidic cations for the binding sites of SOC, which would also have protonated functional groups (Rasmussen et al., 2018; Sowers et al., 2018). Textural differences at our site may have played some role in SOC distribution across the hill slope. Clay content is regularly linked to SOC content, but increased with depth and was thus, negatively related to SOC content in our PCA analysis (Figure 7d). Yet, Core 3 towards the north of our site in the mid-slope had a high clay content throughout all depths and a particularly high SOC content, supporting the idea that depth-resolved variations in clay content may have influenced the distribution of SOC at PRFS. Furthermore, while soil CO_2 fluxes were lower in the down-slope in 2021, the higher rainfall and soil moisture in 2022 ensured that soil CO_2 fluxes were not limited in the down-slope, like other landscape positions. Thus, the depth distribution of clay across our site and higher moisture content down-slope during wetter years may have played some role in governing the distribution of SOC content and contradicting our initial hypothesis.

The observation that SOC was higher in the mid-slope was also contrary to other studies that have investigated the influence of landscape position on grassland SOC dynamics, which tend to find that SOC was lower in the mid-slope and higher in the down-slope (Buraka et al., 2022; Singh & Benbi, 2018). In a study specifically on the grasslands of California in hilly environments, Lin et al. (2016) demonstrated that subsoil thickness had a significant effect on the C stocks. Furthermore, the authors reported that C stocks were higher in convex ridge positions despite their drier conditions than concave or toe slope positions (Lin et al., 2016). While SOC stocks are not the same as SOC content, the observations of Lin et al. (2016) are similar to our own, where SOC content was higher in the zone that dried the quickest. Thereby suggesting that landscape position may have had some influence on the SOC distribution of our California grassland.

Another potential influence on the distribution of SOC at the PRFS could be the belowground inputs of the different dominant grassland species, present at different landscape positions in our site (Figure 5). Grasses allocate *ca*. 90% of C belowground (Bai & Cotrufo, 2022; Jackson et al., 2017; Silver et al., 2010), where it is five times more likely to be preserved than aboveground inputs (Jackson et al., 2017) and can readily contribute to the mineral associated pool (Villarino et al., 2021). *Holcus lanatus* in particular was the dominant species in the mid-slope, where SOC was highest, and it has been demonstrated to have a fast-growing root network (de Vries & Bardgett, 2016) that abundantly allocates SOC to the rhizosphere (Ladygina & Hedlund, 2010) through high rates of exudation (de Vries et al., 2019). Overall, the distribution of SOC is widely accepted to be an emergent property of many different past and present ecosystem properties that evolves through time, including soil texture, moisture, landscape position, and vegetation changes (Kleber et al., 2021; Matteodo et al., 2018; Schmidt et al., 2011). Further studies are now needed to further investigate the influence of these different critical-zone properties on the overall distribution and quality of SOC at the PRFS as well as its response to future change.

7. Conclusions—The Critical-Zone Framework and Future Warming

We completed a multidisciplinary characterisation of a small hillslope at Point Reyes, including above- and below-ground observations, to better understand how landscape position influenced the critical-zone properties of a coastal grassland in California. With geophysical and remote sensing methods, further constrained by plant and soil point measurements, we identified significant spatial and temporal heterogeneity at the site, largely driven by slope and variations in subsurface moisture. Statistical clustering of the various data sets revealed that our site could be broadly split into four environmental zones, which had distinct ecosystem properties and varied with landscape position down the hillslope. Aboveground cultivated biomass was lowest in the up-slope and along

with NDVI values, increased moving downslope where soil moisture content remained higher for longer throughout the dry season. This higher soil moisture content seemed to instigate a dual threshold response on soil CO_2 fluxes; whereby, high moisture inhibited soil CO_2 fluxes in the down-slope during the wet winter months and rain events following the dry summer months enhanced soil CO_2 fluxes. In turn this characterisation has helped to identify heterogeneity that could shape the response of this environment to future ecosystem disturbances such as changes in precipitation, fire, or warming (Figures S16 and S18 in Supporting Information S1). This study highlights that importance of accounting for landscape position when investigating grassland ecosystem functioning and heterogeneity, while creating a novel framework for the combination of multidisciplinary data sets to investigate critical-zone environments.

Data Availability Statement

Data from this manuscript is freely available at ESS-DIVE (https://data.ess-dive.lbl.gov/data) under the identifier: ess-dive-876a09356183149-20240130T090100726.

Acknowledgments
This material is based upon work supported by the Swiss National Science Foundation (Grants P2LAP2_195077 and P500PN_20665) and the Department of Energy, Office of Biological and Environmental Research Science Program under contract number DE-AC02-05CH11231. Use of the Stanford Synchrotron Radiation Lightsource, SLAC National Accelerator Laboratory, is supported by the U.S. Department of Energy, Office of Science, Office of Basic Energy Sciences under Contract No. DE-AC02-76SF00515. We are grateful to beamline scientists and support staff from 11 to 3 at SSRL, including Vivek Thampy, Chris Tassone, and Cathy Knotts. Special thanks to Patricia Fox (LBNL) and Amanda Rodriguez (UC Davis) for their support with certain chemical analyses. Special thanks also to the Point Reyes National Seashore liaison team and the Belowground Biogeochemistry Scientific Focus Area group. We also thank Shelly Benson for conducting the vegetation surveys at the PRFS.

References

Amme, D. (2008). The grasses and grasslands of Marin and Sonoma counties. *Grasslands*, *18*(1), 12–17.
Aran, D., Maul, A., & Masfaraud, J.-F. (2008). A spectrophotometric measurement of soil cation exchange capacity based on cobaltihexamine chloride absorbance. *Comptes Rendus Geoscience*, *340*(12), 865–871. https://doi.org/10.1016/j.crte.2008.07.015
Archie, G. E. (1942). The electrical resistivity log as an aid in determining some reservoir characteristics. *Transactions of the AIME*, *146*(01), 54–62. https://doi.org/10.2118/942054-g
Ata Rezaei, S., & Gilkes, R. J. (2005). The effects of landscape attributes and plant community on soil chemical properties in rangelands. *Geoderma*, *125*(1), 167–176. https://doi.org/10.1016/j.geoderma.2004.07.010
Bai, Y., & Cotrufo, M. F. (2022). Grassland soil carbon sequestration: Current understanding, challenges, and solutions. *Science*, *377*(6606), 603–608. https://doi.org/10.1126/science.abo2380
Bardgett, R. D., Bullock, J. M., Lavorel, S., Manning, P., Schaffner, U., Ostle, N., et al. (2021). Combatting global grassland degradation. *Nature Reviews Earth & Environment*, *2*(10), 720–735. https://doi.org/10.1038/s43017-021-00207-2
Barnard, R. L., Blazewicz, S. J., & Firestone, M. K. (2020). Rewetting of soil: Revisiting the origin of soil CO_2 emissions. *Soil Biology and Biochemistry*, *147*, 107819. https://doi.org/10.1016/j.soilbio.2020.107819
Bengtsson, J., Bullock, J. M., Egoh, B., Everson, C., Everson, T., O'Connor, T., et al. (2019). Grasslands—More important for ecosystem services than you might think. *Ecosphere*, *10*(2), e02582. https://doi.org/10.1002/ecs2.2582
Bennie, J., Huntley, B., Wiltshire, A., Hill, M. O., & Baxter, R. (2008). Slope, aspect and climate: Spatially explicit and implicit models of topographic microclimate in chalk grassland. *Ecological Modelling*, *216*(1), 47–59. https://doi.org/10.1016/j.ecolmodel.2008.04.010
Bense, V. F., Gleeson, T., Loveless, S. E., Bour, O., & Scibek, J. (2013). Fault zone hydrogeology. *Earth-Science Reviews*, *127*, 171–192. https://doi.org/10.1016/j.earscirev.2013.09.008
Birch, H. F. (1958). The effect of soil drying on humus decomposition and nitrogen availability. *Plant and Soil*, *10*(1), 9–31. https://doi.org/10.1007/bf01343734
Bowden, R. D., Nadelhoffer, K. J., Boone, R. D., Melillo, J. M., & Garrison, J. B. (1993). Contributions of aboveground litter, belowground litter, and root respiration to total soil respiration in a temperate mixed hardwood forest. *Canadian Journal of Forest Research*, *23*(7), 1402–1407. https://doi.org/10.1139/x93-177
Brantley, S. L., Goldhaber, M. B., & Vala, R. K. (2007). Crossing disciplines and scales to understand the critical zone. *Elements*, *3*(5), 307–314. https://doi.org/10.2113/gselements.3.5.307
Buraka, T., Elias, E., & Lelago, A. (2022). Soil organic carbon and its' stock potential in different land-use types along slope position in Coka watershed, Southern Ethiopia. *Heliyon*, *8*(8), e10261. https://doi.org/10.1016/j.heliyon.2022.e10261
Carrera-Hernández, J. J., Smerdon, B. D., & Mendoza, C. A. (2012). Estimating groundwater recharge through unsaturated flow modelling: Sensitivity to boundary conditions and vertical discretization. *Journal of Hydrology*, *452–453*, 90–101. https://doi.org/10.1016/j.jhydrol.2012.05.039
Chadwick, O. A., & Chorover, J. (2001). The chemistry of pedogenic thresholds. *Geoderma*, *100*(3–4), 321–353. https://doi.org/10.1016/s0016-7061(01)00027-1
Chambers, J. C., Allen, C. R., & Cushman, S. A. (2019). Operationalizing ecological resilience concepts for managing species and ecosystems at risk. *Frontiers in Ecology and Evolution*, *7*. https://doi.org/10.3389/fevo.2019.00241
Chorover, J., Kretzschmar, R., Garcia-Pichel, F., & Sparks, D. L. (2007). Soil biogeochemical processes within the critical zone. *Elements*, *3*(5), 321–326. https://doi.org/10.2113/gselements.3.5.321
Clark, J. C., & Brabb, E. E. (1997). Geology of Point Reyes national seashore and vicinity, California: A digital database (pp. 97–456).
Council, N. R. (2001). *Basic research opportunities in Earth science*. The National Academies Press.
Dafflon, B., Léger, E., Falco, N., Wainwright, H. M., Peterson, J., Chen, J., et al. (2023). Advanced monitoring of soil-vegetation co-dynamics reveals the successive controls of snowmelt on soil moisture and on plant seasonal dynamics in a mountainous watershed. *Frontiers in Earth Science*, *11*. https://doi.org/10.3389/feart.2023.976227
Dafflon, B., Oktem, R., Peterson, J., Ulrich, C., Tran, A. P., Romanovsky, V., & Hubbard, S. S. (2017). Coincident aboveground and belowground autonomous monitoring to quantify covariability in permafrost, soil, and vegetation properties in Arctic tundra. *Journal of Geophysical Research: Biogeosciences*, *122*(6), 1321–1342. https://doi.org/10.1002/2016jg003724
Dafflon, B., Wu, Y., Hubbard, S. S., Birkholzer, J. T., Daley, T. M., Pugh, J. D., et al. (2013). Monitoring CO_2 intrusion and associated geochemical transformations in a shallow groundwater system using complex electrical methods. *Environmental Science & Technology*, *47*(1), 314–321. https://doi.org/10.1021/es301260e
D'antonio, C. M., Malmstrom, C., Reynolds, S. A., & Gerlach, J. (2007). Ecology of invasive non-native species in California grasslands. In M. Stromberg (Ed.), *California grasslands: Ecology and management*. University of California Press.

Dass, P., Houlton, B. Z., Wang, Y., & Warlind, D. (2018). Grasslands may be more reliable carbon sinks than forests in California. *Environmental Research Letters*, *13*(7), 074027. https://doi.org/10.1088/1748-9326/aacb39

Devadoss, J., Falco, N., Dafflon, B., Wu, Y., Franklin, M., Hermes, A., et al. (2020). Remote sensing-informed zonation for understanding snow, plant and soil moisture dynamics within a mountain ecosystem. *Remote Sensing*, *12*(17), 2733. https://doi.org/10.3390/rs12172733

de Vries, F. T., & Bardgett, R. D. (2016). Plant community controls on short-term ecosystem nitrogen retention. *New Phytologist*, *210*(3), 861–874. https://doi.org/10.1111/nph.13832

de Vries, F. T., Williams, A., Stringer, F., Willcocks, R., McEwing, R., Langridge, H., & Straathof, A. L. (2019). Changes in root-exudate-induced respiration reveal a novel mechanism through which drought affects ecosystem carbon cycling. *New Phytologist*, *224*(1), 132–145. https://doi.org/10.1111/nph.16001

Eviner, V. T. (2016). Grasslands. In H. Mooney & E. Zavaleta (Eds.), *Ecosystems of California* (pp. 449–478). University of California Press.

Falco, N., Wainwright, H., Dafflon, B., Léger, E., Peterson, J., Steltzer, H., et al. (2019). Investigating microtopographic and soil controls on a mountainous meadow plant community using high-resolution remote sensing and surface geophysical data. *Journal of Geophysical Research: Biogeosciences*, *124*(6), 1618–1636. https://doi.org/10.1029/2018jg004394

Falco, N., Wainwright, H. M., Dafflon, B., Ulrich, C., Soom, F., Peterson, J. E., et al. (2021). Influence of soil heterogeneity on soybean plant development and crop yield evaluated using time-series of UAV and ground-based geophysical imagery. *Scientific Reports*, *11*(1), 7046. https://doi.org/10.1038/s41598-021-86480-z

Fierer, N., Chadwick, O. A., & Trumbore, S. E. (2005). Production of CO_2 in soil profiles of a California annual grassland. *Ecosystems*, *8*(4), 412–429. https://doi.org/10.1007/s10021-003-0151-y

Fissore, C., Dalzell, B. J., Berhe, A. A., Voegtle, M., Evans, M., & Wu, A. (2017). Influence of topography on soil organic carbon dynamics in a Southern California grassland. *CATENA*, *149*, 140–149. https://doi.org/10.1016/j.catena.2016.09.016

Friedman, S. P. (2005). Soil properties influencing apparent electrical conductivity: A review. *Computers and Electronics in Agriculture*, *46*(1–3), 45–70. https://doi.org/10.1016/j.compag.2004.11.001

Frischnecht, F. C. (1987). Electromagnetic physical scale modelling. In *Electromagnetic methods applied geophysical theory* (pp. 365–441).

Galecki, A., & Burzykowski, T. (2015). *Linear mixed-effects models using R: A step-by-step approach*. Springer.

Galloway, A. J. (1977). *Geology of the Point Reyes Peninsula, Marin County, California*. California Division of Mines and Geology.

Harris, P., Bol, R., Evans, J., Hawkins, J. M. B., Dixon, E. R., Wolf, K., et al. (2018). Effect of long-term drainage on plant community, soil carbon and nitrogen contents and stable isotopic ($\delta^{13}C$, $\delta^{15}N$) composition of a permanent grassland. *European Journal of Soil Science*, *69*(1), 48–68. https://doi.org/10.1111/ejss.12504

Hawkesford, M., Horst, W., Kichey, T., Lambers, H., Schjoerring, J., Møller, I. S., & White, P. (2012). Chapter 6 - Functions of macronutrients. In P. Marschner (Ed.), *Marschner's mineral nutrition of higher plants* (3rd ed., pp. 135–189). Academic Press.

Hayley, K., Bentley, L. R., Gharibi, M., & Nightingale, M. (2007). Low temperature dependence of electrical resistivity: Implications for near surface geophysical monitoring. *Geophysical Research Letters*, *34*(18). https://doi.org/10.1029/2007gl031124

Hermes, A. L., Wainwright, H. M., Wigmore, O., Falco, N., Molotch, N. P., & Hinckley, E.-L. S. (2020). From patch to catchment: A statistical framework to identify and map soil moisture patterns across complex alpine terrain. *Frontiers in Water*, *2*. https://doi.org/10.3389/frwa.2020.578602

Hubbard, S. S., Gangodagamage, C., Dafflon, B., Wainwright, H., Peterson, J., Gusmeroli, A., et al. (2013). Quantifying and relating land-surface and subsurface variability in permafrost environments using LiDAR and surface geophysical datasets. *Hydrogeology Journal*, *21*(1), 149–169. https://doi.org/10.1007/s10040-012-0939-y

Hubbard, S. S., & Rubin, Y. (2005). Introduction to Hydrogeophysics. In Y. Rubin & S. S. Hubbard (Eds.), *Hydrogeophysics* (pp. 3–21). Springer.

Huenneke, L. F. (1989). Distribution and regional patterns of Californian Grasslands. In L. F. Huenneke & H. A. Mooney (Eds.), *Grassland structure and function: California annual grassland* (pp. 1–12). Springer.

Huggett, R. J. (1975). Soil landscape systems: A model of soil Genesis. *Geoderma*, *13*(1), 1–22. https://doi.org/10.1016/0016-7061(75)90035-x

IUSS Working Group WRB. (2015). *World reference base for soil resources 2014, update 2015. No 106*. FAO.

Jackson, R. B., Lajtha, K., Crow, S. E., Hugelius, G., Kramer, M. G., & Piñeiro, G. (2017). The ecology of soil carbon: Pools, vulnerabilities, and biotic and abiotic controls. *Annual Review of Ecology, Evolution, and Systematics*, *48*(1), 419–445. https://doi.org/10.1146/annurev-ecolsys-112414-054234

Jankowska-Huflejt, H. H. (2006). The function of permanent grasslands in water resources protection. *Journal of Water and Land Development*, *10*(1), 55–65. https://doi.org/10.2478/v10025-007-0005-7

Jantz, P. A., Preusser, B. F. L., Fujikawa, J. K., Kuhn, J. A., Bersbach, C. J., Gelbard, J. L., & Davis, F. W. (2007). Regulatory protection and conservation. In M. R. Stromberg, C. J. D, & D. A. Carla (Eds.), *California grasslands: Ecology and management*. University of California Press.

Keiluweit, M., Wanzek, T., Kleber, M., Nico, P., & Fendorf, S. (2017). Anaerobic microsites have an unaccounted role in soil carbon stabilization. *Nature Communications*, *8*(1), 1771. https://doi.org/10.1038/s41467-017-01406-6

Kleber, M., Bourg, I. C., Coward, E. K., Hansel, C. M., Myneni, S. C. B., & Nunan, N. (2021). Dynamic interactions at the mineral–organic matter interface. *Nature Reviews Earth & Environment*, *2*(6), 402–421. https://doi.org/10.1038/s43017-021-00162-y

Kumar, L., Skidmore, A. K., & Knowles, E. (1997). Modelling topographic variation in solar radiation in a GIS environment. *International Journal of Geographical Information Science*, *11*(5), 475–497. https://doi.org/10.1080/136588197242266

Ladygina, N., & Hedlund, K. (2010). Plant species influence microbial diversity and carbon allocation in the rhizosphere. *Soil Biology and Biochemistry*, *42*(2), 162–168. https://doi.org/10.1016/j.soilbio.2009.10.009

Likens, G. E., Driscoll, C. T., Buso, D. C., Siccama, T. G., Johnson, C. E., Lovett, G. M., et al. (1994). The biogeochemistry of potassium at Hubbard Brook. *Biogeochemistry*, *25*(2), 61–125. https://doi.org/10.1007/bf00000881

Lin, Y., Prentice, S. E., Tran, T., Bingham, N. L., King, J. Y., & Chadwick, O. A. (2016). Modeling deep soil properties on California grassland hillslopes using LiDAR digital elevation models. *Geoderma Regional*, *7*(1), 67–75. https://doi.org/10.1016/j.geodrs.2016.01.005

Liu, D., Zhang, C., Ogaya, R., Fernández-Martínez, M., Pugh, T. A. M., & Peñuelas, J. (2021). Increasing climatic sensitivity of global grassland vegetation biomass and species diversity correlates with water availability. *New Phytologist*, *230*(5), 1761–1771. https://doi.org/10.1111/nph.17269

Livingston, D. S. (1995). A good lift: Dairy farming in the Olema Valley. In *National park service historical resource study, Marin County*.

Matteodo, M., Grand, S., Sebag, D., Rowley, M. C., Vittoz, P., & Verrecchia, E. P. (2018). Decoupling of topsoil and subsoil controls on organic matter dynamics in the Swiss Alps. *Geoderma*, *330*, 41–51. https://doi.org/10.1016/j.geoderma.2018.05.011

McLachlan, P., Blanchy, G., & Binley, A. (2021). EMagPy: Open-source standalone software for processing, forward modeling and inversion of electromagnetic induction data. *Computers & Geosciences*, *146*, 104561. https://doi.org/10.1016/j.cageo.2020.104561

McSherry, M. E., & Ritchie, M. E. (2013). Effects of grazing on grassland soil carbon: A global review. *Global Change Biology*, *19*(5), 1347–1357. https://doi.org/10.1111/gcb.12144
Nolan, M. P. (2021). Restoring native California grasslands in a changing climate.
Novák, V., & Hlaváčiková, H. (2019). *Applied soil hydrology*. Springer.
NRCS, U. (2022). Web soil survey: Soil survey staff. In U. S. D. O. Agriculture (Ed.) *Web Soil Survey*. http://websoilsurvey.nrcs.usda.gov/
Pansu, M., & Gautheyrou, J. (2006). *Handbook of soil analysis: Mineralogical, organic and inorganic methods*. Springer.
Paton, T. R., Humphreys, G. S., & Mitchell, P. B. (1995). *Soils: A new global view*. Yale University Press.
Pedregosa, F., Varoquaux, G., Gramfort, A., Michel, V., Thirion, B., Grisel, O., et al. (2011). Scikit-learn: Machine learning in Python. *Journal of Machine Learning Research*, *12*, 2825–2830.
Phillips, J. D. (2007). Development of texture contrast soils by a combination of bioturbation and translocation. *CATENA*, *70*(1), 92–104. https://doi.org/10.1016/j.catena.2006.08.002
Placella, S. A., Brodie, E. L., & Firestone, M. K. (2012). Rainfall-induced carbon dioxide pulses result from sequential resuscitation of phylogenetically clustered microbial groups. *Proceedings of the National Academy of Sciences of the United States of America*, *109*(27), 10931–10936. https://doi.org/10.1073/pnas.1204306109
Rasmussen, C., Heckman, K., Wieder, W. R., Keiluweit, M., Lawrence, C. R., Berhe, A. A., et al. (2018). Beyond clay: Towards an improved set of variables for predicting soil organic matter content. *Biogeochemistry*, *137*(3), 297–306. https://doi.org/10.1007/s10533-018-0424-3
Rasmussen, C., Troch, P. A., Chorover, J., Brooks, P., Pelletier, J., & Huxman, T. E. (2011). An open system framework for integrating critical zone structure and function. *Biogeochemistry*, *102*(1), 15–29. https://doi.org/10.1007/s10533-010-9476-8
Rousseeuw, P. J. (1987). Silhouettes: A graphical aid to the interpretation and validation of cluster analysis. *Journal of Computational and Applied Mathematics*, *20*, 53–65. https://doi.org/10.1016/0377-0427(87)90125-7
Rowley, M. C., Grand, S., Adatte, T., & Verrecchia, E. P. (2020). A cascading influence of calcium carbonate on the biogeochemistry and pedogenic trajectories of subalpine soils, Switzerland. *Geoderma*, *361*, 114065. https://doi.org/10.1016/j.geoderma.2019.114065
Rowley, M. C., Nico, P. S., Bone, S. E., Marcus, M. A., Pegoraro, E. F., Castanha, C., et al. (2023). Association between soil organic carbon and calcium in acidic grassland soils from Point Reyes National Seashore, CA. *Biogeochemistry*, *165*(1), 91–111. https://doi.org/10.1007/s10533-023-01059-2
Rudolph, S., van der Kruk, J., von Hebel, C., Ali, M., Herbst, M., Montzka, C., et al. (2015). Linking satellite derived LAI patterns with subsoil heterogeneity using large-scale ground-based electromagnetic induction measurements. *Geoderma*, *241–242*, 262–271. https://doi.org/10.1016/j.geoderma.2014.11.015
Ryals, R., Kaiser, M., Torn, M. S., Berhe, A. A., & Silver, W. L. (2014). Impacts of organic matter amendments on carbon and nitrogen dynamics in grassland soils. *Soil Biology and Biochemistry*, *68*, 52–61. https://doi.org/10.1016/j.soilbio.2013.09.011
Sanderman, J., & Amundson, R. (2008). A comparative study of dissolved organic carbon transport and stabilization in California forest and grassland soils. *Biogeochemistry*, *89*(3), 309–327. https://doi.org/10.1007/s10533-008-9221-8
Sanderman, J., & Amundson, R. (2010). Soil carbon dioxide production and climatic sensitivity in contrasting California ecosystems. *Soil Science Society of America Journal*, *74*(4), 1356–1366. https://doi.org/10.2136/sssaj2009.0290
Satterthwaite, F. E. (1946). An approximate distribution of estimates of variance components. *Biometric Bulletin*, *2*(6), 110–114. https://doi.org/10.2307/3002019
Schaetzl, R. J., & Thompson, M. L. (2015). *Soil genesis and geomorphology* (2nd ed.). Cambridge Univeristy Press.
Schimel, J. P., Wetterstedt, J. Å. M., Holden, P. A., & Trumbore, S. E. (2011). Drying/rewetting cycles mobilize old C from deep soils from a California annual grassland. *Soil Biology and Biochemistry*, *43*(5), 1101–1103. https://doi.org/10.1016/j.soilbio.2011.01.008
Schmidt, M. W. I., Torn, M. S., Abiven, S., Dittmar, T., Guggenberger, G., Janssens, I. A., et al. (2011). Persistence of soil organic matter as an ecosystem property. *Nature*, *478*(7367), 49–56. https://doi.org/10.1038/nature10386
Silver, W. L., Ryals, R., & Eviner, V. (2010). Soil carbon pools in California's annual grassland ecosystems. *Rangeland Ecology & Management*, *63*(1), 128–136. https://doi.org/10.2111/rem-d-09-00106.1
Singh, P., & Benbi, D. K. (2018). Soil organic carbon pool changes in relation to slope position and land-use in Indian lower Himalayas. *CATENA*, *166*, 171–180. https://doi.org/10.1016/j.catena.2018.04.006
Skopp, J., Jawson, M. D., & Doran, J. W. (1990). Steady-state aerobic microbial activity as a function of soil water content. *Soil Science Society of America Journal*, *54*(6), 1619–1625. https://doi.org/10.2136/sssaj1990.03615995005400060018x
Slessarev, E. W., Lin, Y., Bingham, N. L., Johnson, J. E., Dai, Y., Schimel, J. P., & Chadwick, O. A. (2016). Water balance creates a threshold in soil pH at the global scale. *Nature*, *540*(7634), 567–569. https://doi.org/10.1038/nature20139
SoilWeb. (2021). Web soil survey: Soil survey staff, natural resources conservation service. In U. S. D. O. A. A. U. C. Davis (Ed.). *Web Soil Survey*.
Sowers, T. D., Stuckey, J. W., & Sparks, D. L. (2018). The synergistic effect of calcium on organic carbon sequestration to ferrihydrite. *Geochemical Transactions*, *19*(1), 4. https://doi.org/10.1186/s12932-018-0049-4
Stromberg, M., Kephart, P., & Yadon, V. (2001). Composition, invisibility, and diversity in coastal California grasslands. *Madroño*, *48*, 236–252.
Stromberg, M. R., D, C. J., & Carla, D. A. (Eds.) (2007)., *California grasslands: Ecology and management*. University of California Press.
Sumner, M. E. (1994). Measurement of soil pH: Problems and solutions. *Communications in Soil Science and Plant Analysis*, *25*(7–8), 859–879. https://doi.org/10.1080/00103629409369085
Suttie, J., Reynolds, S., & Batello, C. (2005). Grasslands of the World.
Thompson, J. A., Bell, J. C., & Zanner, C. W. (1998). Hydrology and hydric soil extent within a Mollisol catena in southeastern Minnesota. *Soil Science Society of America Journal*, *62*(4), 1126–1133. https://doi.org/10.2136/sssaj1998.03615995006200040038x
van Reeuwijk, L. P. (2002). *Procedures for soil analysis* (6th ed.). FOA - Food and Agriculture Organization of United Nations: International soil reference and information center (ISRIC).
Villarino, S. H., Pinto, P., Jackson, R. B., & Piñeiro, G. (2021). Plant rhizodeposition: A key factor for soil organic matter formation in stable fractions. *Science Advances*, *7*(16), eabd3176. https://doi.org/10.1126/sciadv.abd3176
von Hebel, C., Matveeva, M., Verweij, E., Rademske, P., Kaufmann, M. S., Brogi, C., et al. (2018). Understanding soil and plant interaction by combining ground-based quantitative electromagnetic induction and airborne hyperspectral data. *Geophysical Research Letters*, *45*(15), 7571–7579. https://doi.org/10.1029/2018gl078658
Wainwright, H. M., Dafflon, B., Smith, L. J., Hahn, M. S., Curtis, J. B., Wu, Y., et al. (2015). Identifying multiscale zonation and assessing the relative importance of polygon geomorphology on carbon fluxes in an Arctic tundra ecosystem. *Journal of Geophysical Research: Biogeosciences*, *120*(4), 788–808. https://doi.org/10.1002/2014jg002799

Wainwright, H. M., Oktem, R., Dafflon, B., Dengel, S., Curtis, J. B., Torn, M. S., et al. (2021). High-resolution spatio-temporal estimation of net ecosystem exchange in ice-wedge polygon tundra using in situ sensors and remote sensing data. *Land*, *10*(7), 722. https://doi.org/10.3390/land10070722

Wainwright, H. M., Steefel, C., Trutner, S. D., Henderson, A. N., Nikolopoulos, E. I., Wilmer, C. F., et al. (2020). Satellite-derived foresummer drought sensitivity of plant productivity in Rocky Mountain headwater catchments: Spatial heterogeneity and geological-geomorphological control. *Environmental Research Letters*, *15*(8), 084018. https://doi.org/10.1088/1748-9326/ab8fd0

Wainwright, H. M., Uhlemann, S., Franklin, M., Falco, N., Bouskill, N. J., Newcomer, M. E., et al. (2022). Watershed zonation through hillslope clustering for tractably quantifying above- and below-ground watershed heterogeneity and functions. *Hydrology and Earth System Sciences*, *26*(2), 429–444. https://doi.org/10.5194/hess-26-429-2022

Wang, J., Epstein, H. E., & Wang, L. (2010). Soil CO_2 flux and its controls during secondary succession. *Journal of Geophysical Research*, *115*(G2), G02005. https://doi.org/10.1029/2009jg001084

White, R. P., Murray, S., Rohweder, M., Prince, S., & Thompson, K. (2000). *Grassland ecosystems*. World Resources Institute.

Xiang, S.-R., Doyle, A., Holden, P. A., & Schimel, J. P. (2008). Drying and rewetting effects on C and N mineralization and microbial activity in surface and subsurface California grassland soils. *Soil Biology and Biochemistry*, *40*(9), 2281–2289. https://doi.org/10.1016/j.soilbio.2008.05.004

Zhao, G. (2022). Trends in grassland science: Based on the shift analysis of research themes since the early 1900s. *Fundamental Research*, *3*(2), 201–208. https://doi.org/10.1016/j.fmre.2022.05.008

References From the Supporting Information

Thampy, V. (2021). xdart, Stanford Synchrotron Radiation Lightsource.